LA-UR- 97-4835

Title: TWO WIDE-ANGLE IMAGING NEUTRAL-ATOM SPECTROMETERS

Author(s): David J. McComas

Submitted to: Informal Distribution

Los Alamos
NATIONAL LABORATORY

Form No. 836 R5
ST 2629 10/91

DISCLAIMER

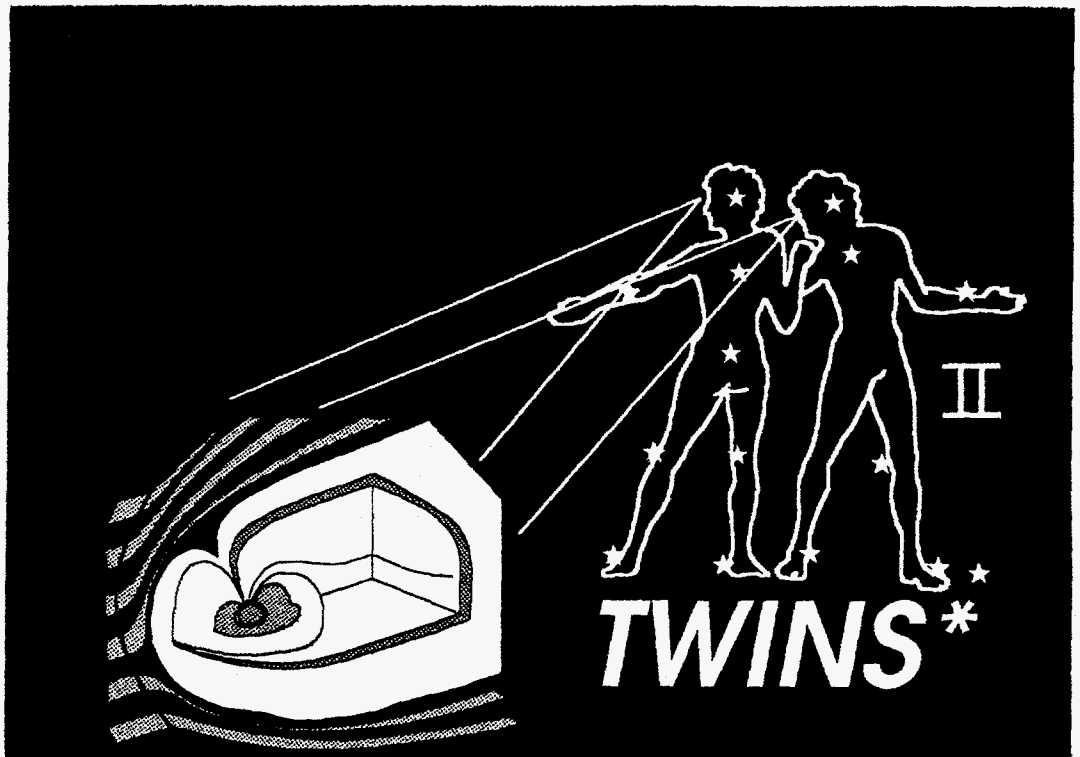

*Two Wide-Angle Imaging Neutral-Atom Spectrometers

Dr. David J. McComas, Principal Investigator,
Los Alamos National Laboratory, Los Alamos, NM 87545

Principal Investigator

David J. McComas
Los Alamos National Laboratory
P.O. Box 1663, MS D466
Los Alamos, NM 87545
Phone: 505-667-0138, Fax 505-665-7395
E-Mail: dmccomas@lanl.gov

Laboratory Coordinator for NASA Programs

S. Peter Gary
Los Alamos National Laboratory
P.O. Box 1663, MS D466
Los Alamos, NM 87545
Phone: 505-667-3807, Fax 505-665-7395
E-Mail: dmccomas@lanl.gov

TABLE OF CONTENTS

1.0 SCIENCE

1.1 Science Goals and Objectives

The Two Wide-angle Imaging Neutral-atom Spectrometers (TWINS) mission provides a new capability for stereoscopically imaging the magnetosphere. By imaging the charge exchange neutral atoms over a broad energy range (1<E<~100 keV) using two identical instruments on two widely-spaced high-altitude, high-inclination spacecraft (Figure 1.1), TWINS will enable the 3-dimensional visualization and the resolution of large scale structures and dynamics within the magnetosphere for the first time. These observations will provide a leap ahead in our understanding of the global aspects of the terrestrial magnetosphere and directly address a number of critical issues in the "Sun-Earth Connections" science theme of the NASA Office of Space Science.

1.1.1 Background and Overview

The feasibility of magnetospheric imaging using energetic neutral atoms (ENAs), which arise from the charge exchange process between cold geocoronal neutral hydrogen and the local energetic ion populations, was first demonstrated a decade ago [Roelof, 1987]. Since then, technologies have been developed to provide higher sensitivity, better angular resolution, and, most importantly, to extend the observable ENA energy range downward below several tens of keV to ~1 keV [McComas et al., 1991; 1997]. Recent higher energy neutral atom images from NASA's POLAR spacecraft have provided further tantalizing glimpses of the power of neutral atom imaging (e.g., see the cover article of the 15 May 1997 GRL [Henderson et al., 1997]).

The IMAGE mid-sized Explorer will provide NASA's first dedicated platform for making ENA measurements of the terrestrial magnetosphere. IMAGE, scheduled to launch in January, 2000, is presently under development by a team of researchers including nearly all of the TWINS investigators and led by TWINS Co-I, Dr. J. Burch. TWINS will extend our understanding of magnetospheric structure and processes well beyond what is achievable from IMAGE by providing simultaneous images from two widely separated locations over a broad ENA energy range.

In 1996, NASA released an Announcement of Opportunity to study advanced mission concepts which would be suitable for future Sun-Earth Connections missions. One of the winners of that competition was the MRI-VIDEOS which proposed to study the next logical step in magnetospheric imaging: Stereo imaging of the magnetosphere. The MRI VIDEOS PI (Dr. D. Mitchell) as well as several Co-Is of that study are investigators on TWINS; the TWINS concept and proposed mission have benefited substantially from the MRI-VIDEOS study. Many of the concepts and scientific goals given below are closely related to or taken directly from that proposal and mission study. Finally, the MRI-VIDEOS study has convinced the scientific community of the value of such a mission, and the recent Sun-Earth Connections roadmap explicitly included a dedicated "Stereo Magnetospheric Imager" mission in its Solar-Terrestrial Probes mission set [Burch et al., 1997].

It is very significant that the proposed TWINS mission will provide closure on a large fraction of the MRI-VIDEOS and Stereo Magnetospheric Imager science in a mission of opportunity for a small fraction of the cost of an independent stereo imaging mission. This cost savings is enabled in TWINS by two factors. First, the TWINS instrumentation is essentially the same as that developed for the IMAGE mission. This instrumentation consists of a neutral atom imager covering the 1–100 keV energy range with 4°x4° angular resolution and 1-minute time resolution, and a Lyman-α imager to monitor the geocorona. Second, TWINS will fly as a mission of opportunity on two high-inclination, high altitude spacecraft provided by a non-NASA US organization. For the purposes of this proposal we will simply refer to these spacecraft as S/C-1 and S/C-2. The scientific instrumentation on these spacecraft includes a 50 eV–30 keV plasma analyzer and a >50 keV energetic particle spectrometer/dosimeter. Each spacecraft will be 3-axis stabilized and approximately nadir pointing, and will be placed in a Molniya orbit with 63.4° inclination and 7.2 R_E apogee. A sketch of the two spacecraft orbits is shown in Figure 1.1. The orbits of these spacecraft are ideal for a magnetospheric imaging mission, providing a unique opportunity to obtain stereo images of the

magnetosphere in the near future at low cost. S/C-1 will launch in late 2001 or early 2002 while S/C-2 will launch in late 2003 or early 2004. Once launched, S/C-1 and -2 will be given international designators, and all data will be made available for normal scientific data analysis, educational, and public outreach purposes. Depending on the exact TWINS timing and the duration of the IMAGE science phase, S/C-1 may overlap with the IMAGE mission, providing the first magnetospheric stereo images as early as 2001 or 2002. In any case, however, S/C-1 and -2 will provide a full two year stereo mission beginning in late 2003 or early 2004.

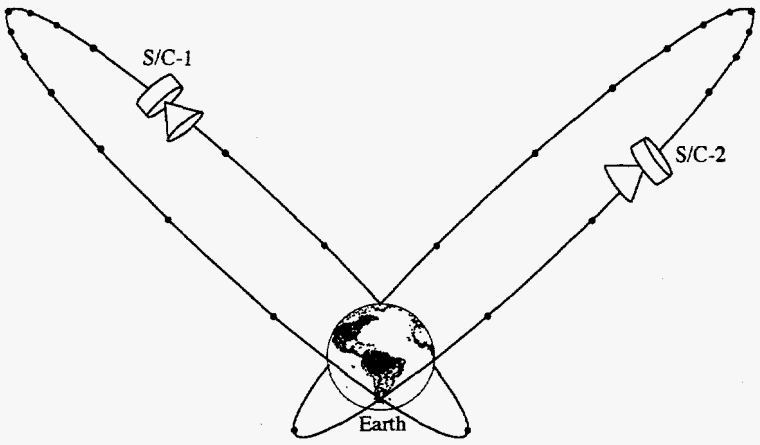

Figure 1.1 The Molniya orbits of the two TWINS spacecraft.

1.1.2 TWINS Scientific Goals

While TWINS has numerous scientific goals that relate to the various individual regions that will be imaged, **the primary scientific goal of the TWINS investigation is to establish the global connectivities and causal relationships between processes in different regions of the magnetosphere.** While the IMAGE MIDEX mission will take the first important step in imaging the magnetosphere, TWINS will advance another major step forward by providing the capability to unfold the emission variation along the line-of-sight from the integrated ENA intensities obtained from each of the spacecraft. The stereo imaging of TWINS will counter a serious difficulty regarding magnetospheric imaging, that of interpreting structures viewed in an optically thin medium, and will greatly reduce the reliance on models for retrieving the three-dimensional magnetospheric structure and dynamics from the data.

The broad scientific objectives of TWINS are listed here. They build on the scientific objectives that have previously been established for NASA's IMAGE mission, and will provide a far less model-dependent path to achieving these goals. The TWINS investigation measurement goals are:

(1) Ion Dynamics: To view the global dynamics, composition, and energization of ions throughout the magnetosphere with approximately one minute time resolution using simultaneously obtained multi-vantage point images of key magnetospheric components including the ring current, inner plasma sheet, near-Earth cross-tail current sheet, the high latitude, low altitude extensions of these regions and of the outer magnetosphere, the magnetotail, boundary layers, and cusp.

(2) Plasma Origins and Destinies: To trace the sources, transport, and sinks of plasma populations, including solar wind entry at the magnetopause, boundary layer flows and convection patterns, acceleration and heating in the near-Earth plasma sheet, and acceleration of ionospheric plasma in the polar regions.

(3) Magnetospheric Evolution: To observe the evolution of the global magnetospheric structure as solar wind coupling and internal processes change the state of the magnetosphere from quiescence, through moderate (substorms) or extreme (storms) levels of activity, to relaxation and a return to quiescence.

(4) Magnetospheric Structure: To visualize and map the global configuration and organization of the magnetosphere in three dimensions using stereo imaging, forward modeling, and image inversion.

These measurement goals will provide the inputs required to establish the spatial connections and temporal causalities between the various magnetospheric components and regions for both active and inactive states of the magnetosphere. For example, the location in the near-Earth magnetotail current sheet where substorm current disruptions initiate remains elusive, and the timing, as well as the mapping, between the equatorial plane and the auroral zone is still unknown. Multi-point imaging holds our best hope for finally resolving these fundamental and long-standing problems by: 1) providing a framework for understanding the role of localized processes in establishing the global magnetospheric configuration and dynamics, and 2) allowing us to extract quantitative information about the configuration and evolution of global electromagnetic parameters, such as the electric field configurations of the inner magnetosphere and the generation of the region 2 magnetic field aligned current system.

Unlike past attempts to achieve these goals via in situ multi-spacecraft studies, stereo magnetospheric imaging provides global, not local observations. Local observations are limited by spacecraft positions which 1) often miss critical phenomena by not being in just the 'right' place, 2) achieve a good spacecraft configuration for only part of an event, and 3) have ambiguity in the timing between events in different regions. In contrast, TWINS will provide nearly continuous, global stereo coverage of the magnetosphere.

The above discussion emphasizes the connectivity and causality aspects of the TWINS science goals. In addition to these global science goals, TWINS will also address detailed science issues within the various observed regions:

Region 2 Currents Despite their obvious importance to global magnetospheric interactions, we are remarkably ignorant of the global and mesoscale configuration and dynamics of the plasma sheet and ring current populations. Deficiencies in our knowledge of their configurations as they relate to models of region 2 current generation have been noted [Lui et al., 1994]. Also, the first published ENA image [Roelof, 1987] exhibited a dramatic day/night asymmetry which was shown to be capable of driving field aligned currents with the same morphology as the region 2 currents [Roelof, 1989]. Is this new scenario correct? How is such a distribution generated, and how is it maintained so that a quasi-stationary region 2 current system results?

Ring Current A scientific understanding of ring-current physics revolves around three elements: injection, evolution, and decay [e.g., Jordanova et al., 1996]. With a significantly improved ability to unfold global ENA images, the stereo imaging from TWINS promises progress in all three areas. First, TWINS will greatly reduce spatial and temporal uncertainties regarding the location and extent of ring-current injections and their relationship to substorms. TWINS will also permit us to follow the global progress of the redistribution of the ring-current ions. Moreover, TWINS allows a direct observation of one of the primary ring-current loss mechanisms, namely charge-exchange with exospheric neutrals. Thus, TWINS will enable us to test directly and quantitatively our understanding of the role of charge-exchange in ring-current decay, including the temporal sequence and spatial distribution. Moreover, with their modest composition capability, sufficient to distinguish the major ring-current constituents, O^+ and H^+, the TWINS ENA imagers can help resolve issues regarding the spatial and temporal dependence of ring-current composition. TWINS offers the opportunity to examine globally the relationship between the level of geomagnetic activity and ring-current composition below 100 keV, in addition to direct observation of charge-exchange loss rates for the two species.

Plasma Sheet Mapping of the ion plasma sheet from the equatorial plane to lower altitudes in the auroral zone will be accomplished through stereographic imaging of the horns of the plasma sheet. The azimuthal structure of these horns and the variation of their size and shape with geomagnetic activity will provide important insight into auroral energization processes and the 3D distribution of Birkeland currents in the nightside magnetosphere. The visualization of the 3D spatial and temporal structure of the high latitude extension of the plasma sheet will be strongly advanced through the application of TWINS multi point observation techniques. In addition to the high-latitude extension of the plasma sheet, TWINS offers the opportunity to directly visualize substorm ion injections and their spatial and temporal progression.

Furthermore, the TWINS compositional capability and reduced spatial ambiguities may enable the exploration of the role of heavy-ion enhancements in multiple substorm initiation [e.g. Baker et al., 1982].

Visualization of the ring current plasma injection, the evolution of the plasma sheet size and location, and the plasma sheet extension to high latitudes will allow direct global observation of the transfer of energy from the magnetotail into the earth's upper atmosphere for the first time. Multipoint stereo imaging will not only enable more robust unfolding of the ion fluxes in these regions, but will also provide more robust and frequent viewing of any given region of interest.

Because the inherent difficulty in inverting single perspective line-of-sight-integrated images will be greatly ameliorated, the science return from the stereo images of the TWINS mission will be much greater than what could be obtained from any single vantage point. We believe the images obtained by TWINS will revolutionize the study of the magnetosphere. However, the most important contribution to magnetospheric science that is offered by multipoint magnetospheric imaging from TWINS is its ability to unambiguously determine the connectivity and causal relationships between the different regions, by locating the ENA emission regions with a precision not possible from a single vantage point.

One additional TWINS science objective is made possible by the inclusion of a Lyman-α imager as part of the TWINS instrument. As shown in the discussion below, knowledge of the H-atom geocoronal density is essential to the unfolding of the ion intensity from the measurement of the ENA intensity. The observational basis for current geocoronal density models is not extensive. One commonly used model is the Chamberlin-type exosphere derived from a four year average of Lyman-α observations from the DE-1 spacecraft [Rairden et al., 1986]. The inclusion of a simple Lyman-α imager on TWINS allows us to monitor the shape and intensity of the geocoronal emissions, providing the knowledge of the neutral-H exosphere needed for unfolding the ENA images, and simultaneously providing valuable information in its own right regarding the spatial and temporal behavior of the neutral exosphere.

1.1.3 TWINS Mission Timing and the Solar Activity Cycle

The TWINS mission, with planned launches of the two TWINS in approximately late 2001 and late 2003, covers the immediate post-maximum phase of Solar Cycle 23. For this cycle, sunspot maximum is predicted for 2000 [Joselyn et al., 1997]. Historically, geomagnetic activity remains high for several years after sunspot maximum. Thus, during the first two years of the TWINS mission (2002 and 2003), the magnetosphere is expected to be near maximum activity. If the NASA IMAGE mission, scheduled for launch in 2000, is extended two years beyond its 2-year prime mission, then the ENA cameras on IMAGE and TWINS S/C-1 will provide stereo ENA viewing for the two years of maximum geomagnetic activity. During 2004 and 2005 when both TWINS are in orbit providing stereo ENA viewing, the predicted geomagnetic activity is expected to have dropped somewhat, but should still be well above minimum. The timing of the TWINS mission is thus nearly optimal for obtaining stereo observations of the active magnetosphere with inter-calibrated ENA cameras.

1.1.4 Imaging Analysis, Inversion, and Unfolding

1.1.4.1 ENA Image Inversion

The TWINS imagers measure the fluxes of ENAs along two independent lines of sight as indirect measurements of the energetic ions. Image inversion is needed to determine the behavior of the ion populations from the ENA images. The basic equation for high-altitude ENA imaging was given by Roelof [1987]:

$$j_{ENA}(\mathbf{r},E,\hat{\mathbf{u}}) = \sigma(E)\int dx\, n_H(\mathbf{r}-\hat{\mathbf{u}}x)\, j_{ion}(\mathbf{r}-\hat{\mathbf{u}}x,E,\hat{\mathbf{u}}) \qquad (1.1)$$

where j_{ENA} and j_{ion} are the unidirectional differential intensities (/cm^2 s sr keV) for the ENA and corresponding singly charged ion species, respectively, at position $\mathbf{r}$ with energy E and velocity direction unit vector $\hat{\mathbf{u}}$, σ is the charge-exchange cross-section, n_H is the density (cm^{-3}) of the H-atom geocorona, and x is the distance along the line of sight (LOS) defined by the ENA direction $\hat{\mathbf{u}}$. By analogy to optical

imaging, we say that the ENA emission is "optically thin" because no additional charge exchanges typically occur between the point of formation of the ENA and the camera location in the rarefied medium of the magnetosphere. The goal of the inversion process is the unfolding of the ion intensity j_{ion} from the LOS integral (weighted by the geocoronal density n_H) when the measured quantity is the intensity j_{ENA} derived from the camera pixel containing the ENA direction $\hat{\mathbf{u}}$.

The availability of multiple viewpoints suggests the application of tomographic techniques, but direct tomographic inversion of Eq. 1.1 would require such a large number of vantage points to obtain a unique solution that it is not presently feasible for magnetospheric applications. Fortunately, alternative inversion techniques exist, based on the application of 'forward models' to discrete data sets. These require smaller data samples, but rely on external constraints derived from physical models. These tools, including automated image unfolding algorithms, have been developed over the last decade for extracting parameters from ENA images [Chase and Roelof, 1995; Roelof et al., 1993; Roelof, 1997]. As part of the MRI-VIDEOS project, we are presently combining them with more general tomographic concepts to develop a hybrid inversion technique that will optimize the extraction of information from simultaneous stereo images.

Image interpretation based on Eq. 1.1 is far less model-dependent for TWINS than for any single platform imager, owing to the additional constraints imposed on the function j_{ion} by multi-point viewing. Stereo viewing will vastly improve the determination of such basic parameters as the L-shell which dominates the emission, the azimuthal distribution of plasma along the L-shell, and the pitch-angle distribution of the energetic ions. In fact, the optically thin nature of the emission becomes a distinct advantage, since the entire three dimensional volume will be simultaneously sampled from two independent viewpoints.

Figure 1.2 illustrates the information that can be extracted with line-of sight integration inversion from a single position. This figure illustrates a model ring current image (above, left), and its MLT vs. L structure (above, right). The ion distribution recovered from forward modeling of the input ring current image is shown below. Although the general morphology is recovered (noon-midnight and dawn-dusk asymmetry), much of the structure in the weaker emission regions is lost. Multi-point imaging would provide the information necessary to retrieve that structure.

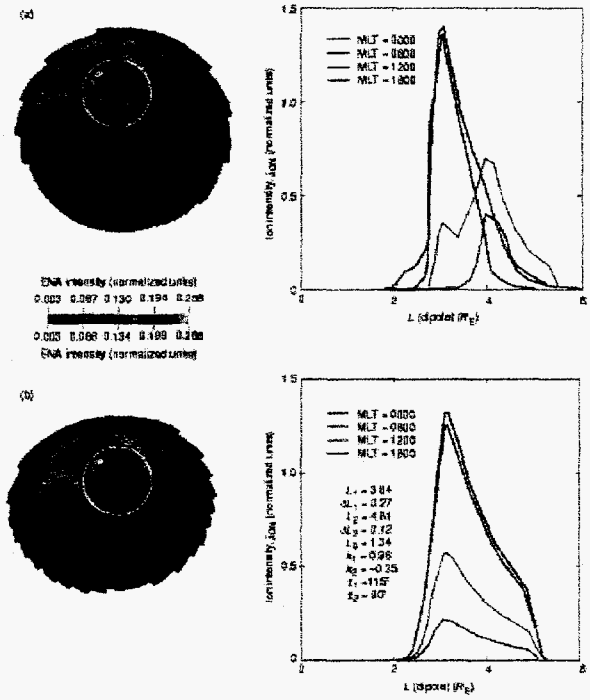

Fig. 1.2 Model ring current input (above) and retrieved (below), using simple forward modeling from a single viewpoint. From Roelof et al. [1993]

Figures 1.3 and 1.4 provide a very striking illustration for why multi-point imaging (as will be done by TWINS) is so valuable. These figures show simulated TWINS images from four geomagnetic latitudes that approximate the dawn sector of the Molniya orbits shown in Fig. 1.1. Counts of 10-20keV H per 4°x4° pixel (including Poisson statistics for a single 60s scan) are color-scaled. The substorm injection of 31 July 1997 observed on POLAR in the midnight sector (4<L<8) by Henderson et al. [1997] is modeled with two pitch-angle distributions (PAD): isotropic, except for empty loss cones (Fig. 1.3) and trapped, with $\sin^{10}\alpha$ (Fig. 1.4). The view from near apogee (lower right panels) shows the midnight location of the energetic ion distribution, but superimposes the emission from all L-shells. However, the oblique views from a lower altitude (45° where Polar was, lower left panels) reveal a distinct difference between the two PADs, because emission from the northern flux tube predominates for the trapped distribution (consistent with the much cruder Polar image). The equatorial view (upper right panels) clearly identifies the trapped PAD by the confinement of its ENA emission to near the equator (as opposed to the isotropic PAD filling the entire flux tubes). The occulation by the Earth limb of the views from southern latitudes approaching perigee (-45°, upper left panel) probes the differences with the maximal spatial resolution acheivable in the orbit. Clearly any pair of these one-minute TWINS exposures obtained simultaneously increases tremendously the effectiveness of the constraints placed on the spatial and pitch-angle dependence of the ion intensity.

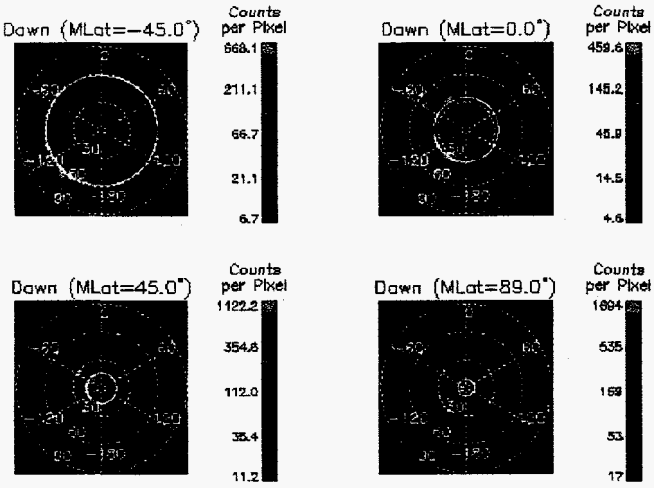

Fig. 1.3 Simulated ENA images from four geomagnetic latitudes (–45°,0°,+45°,+90°) for one of the Molniya orbits shown in Fig. 1.1. A night-side ion injection observed by Polar [Henderson et al., 1997] is modeled with an isotropic pitch-angle distribution.

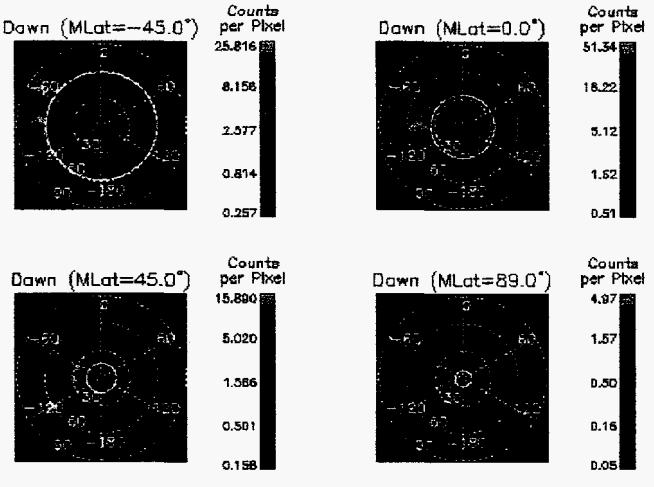

Fig. 1.4 Same as Fig. 1.3, but for a trapped ($\sin^{10}\alpha$) pitch-angle distribution. Because of the emission geometry, only one side of the flux tubes is predominantly illuminated in ENA. Statistics are satisfactory to define the essentials of the morphology, even from apogee.

The inversion (or perhaps more accurately "unfolding") of ENA images to extract quantitative information about the magnetospheric ion population is model-dependent. In principle, the task is to try to infer the six dimensional ion flux $j_{ion}(\mathbf{r},E,\hat{\mathbf{u}})$ in Equation 1.1 for each species from the observed ENA fluxes. This task is made more tractable by symmetries of the physical distribution functions and by magnetospheric ordering. Specifically, Liouville's theorem, combined with the gyrotropic nature of the ion distributions and the conservation of the magnetic moment, reduces the number of independent variables controlling the distributions by two. Thus, since the species and energy are directly measured by the TWINS ENA imager, the flux that must be modeled is a function of only three variables: the MacIlwain parameter L, the magnetic local time Φ, and the equatorial pitch angle α. If the pitch angle distribution is nearly isotropic, as is often the case during high geomagnetic activity [Fok et al., 1996], then the distribution that must be modeled is the 2-D equatorial ion flux $j_{eq}(L,\Phi)$. The availability of two or more viewpoints from stereo imagers then places very strong constraints on the model flux and enables the extraction of quantitative information about the global distribution of magnetospheric ions.

1.1.4.2 Volume Sampling

The center of every pixel of an imager defines a line of sight (LOS) that passes through the magnetosphere. We have argued that the irreducible spatial coordinates are L and Φ, so we now study the way an image is formed in this 2-D space. Figure 1.5a shows a mapping into L-Φ space of LOS curves taken uniformly over 4π sr for pixels 15° in spacecraft elevation by 15° in spacecraft azimuth. The nominal domain of the ring current 3<L<7 is also shown. The spacecraft location in solar magnetic (SM) coordinates is [-1.72,2.82,3.53] R_E, a position on the edge of the polar cap along a Molniya orbit at L=10 and 20 h MLT (Φ =120°). The symbols mark the position of maximum neutral hydrogen density along the LOS (where ENA emission would be brightest if the ion intensity did not also vary) and indicate the magnetic latitude Λ at that point with different symbols: "+" for 0<|Λ|<15°, "x" for 15°<|Λ|<30°, and then squares, diamonds, triangles, and asterisks for each additional 15° in latitude. Another important spatial point along the LOS is the minimum L-value, or the turning point of the curve, where the LOS is tangent to an L-shell, tending to enhance the contribution from that L-shell. These turning points (at L_{min}) are plotted in Figure 1.5b, using the same symbols to indicate the magnetic latitude of the turning point (so that, for example, the "+" symbols show turning points near the magnetic equatorial plane). The angular sampling is now taken at 5° x 5°, the approximate angular resolution of a TWINS camera.

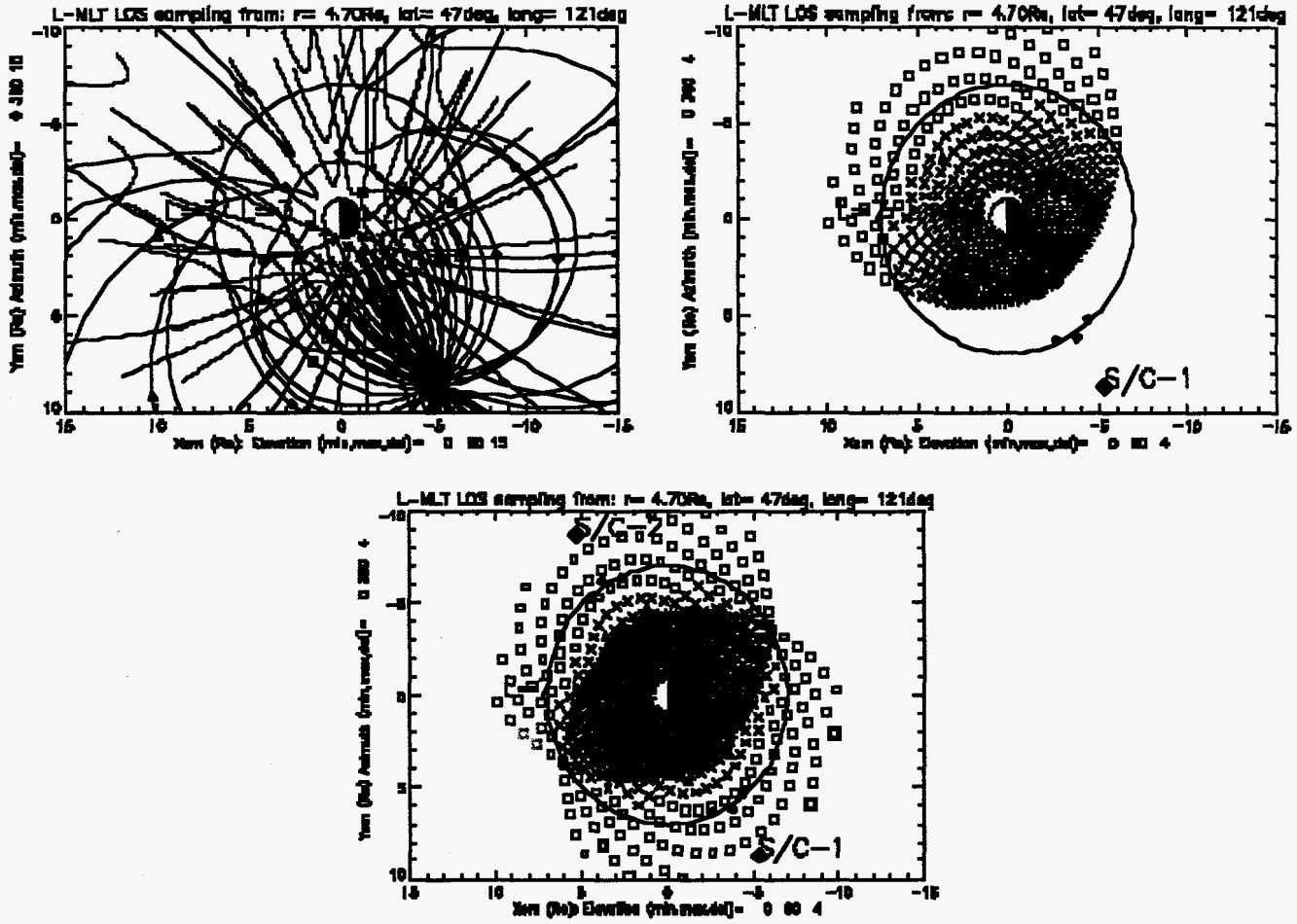

Fig. 1.5 a) Mapping of the pixel LOS for the TWINS FOV in L-MLT coordinates. Each curve (on 15°x15° centers) shows the region of the magnetosphere sampled in ENA. Symbols (see text) mark the position along each LOS of maximum geocoronal density. b) Mapping from Fig. 1.5a of LOS turning points (minimum L) sampled every 4°x4° (TWINS angular resolution). c) Same as Fig 1.5b, but with coverage from TWINS S/C-2 on the opposite side of the polar cap.

What stands out in Figs. 1.5a and b is the dense LOS sampling of the ring current domain 3<L<7 in the quadrant occupied by the spacecraft. This dense sampling is mathematically essential for the stability and uniqueness of any image unfolding algorithm because each LOS constitutes a mathematical constraint on the ion distribution. However, the spacecraft under-samples the other quadrants. The advantage of a stereo mission over a single-spacecraft mission is demonstrated in Fig. 1.5c, which is a superposition of Fig. 1.5b and the corresponding figure for a second spacecraft on the same Molniya orbit at L=10 and Φ=300° (0800 MLT). The sampling of the entire ring current region 3<L<7 is now excellent.

1.1.4.3 Boundary Extraction

One of the goals of the TWINS mission is to image the boundaries between different magnetospheric particle populations. Ion injection boundaries should be visible in the near-Earth plasma sheet when viewed from sufficiently high magnetic latitudes. The ENA images obtained from ISEE-1 [Roelof, 1987] and POLAR [Henderson et al., 1997] are consistent with the boundaries that appear in simulations of ENA images of ion heating of the near-Earth plasma sheet [Hesse et al., 1997]. Another boundary is the magnetopause, or more exactly, the boundary of closed field lines. ENA images should show an edge at the magnetopause whenever energetic ion intensities in the magnetosheath are significantly lower than those of the trapped ions just inside the magnetopause.

Recently Roelof [1997] has developed a model-independent, non-parametric algorithm which extracts the equatorial mapping L(Φ) of an image edge. The algorithm constructs the envelope of all lines-of-sight that view the edge in the image. The algorithm will work for any emission edge formed by an emitting particle population that has a sharp boundary delimited by lines of a known magnetic field, and is robust against Poisson statistical fluctuations in the edge pixels. The LOS envelope forms an outer bound everywhere to the actual boundary .

The edge algorithm is illustrated in Figure 1.6. Fig. 1.6a shows a "wire-model" view of dipole field lines originating at the dayside magnetopause position for an interplanetary dynamical pressure of 2 nPa and B_z=0 [Roelof and Sibeck, 1993]. This "fish-eye" view through the TWINS FOV is from a Molniya orbit near apogee post-midnight at a location [-2.62,-1.84,6.3] R_E in SM coordinates. Applying the algorithm, each LOS tangent to the magnetopause (marked by diamonds) in Fig. 1.6a is mapped onto the L-Φ plane in Fig 1.6b. Their envelope clearly reproduces the location of the dayside magnetopause (shown by the dotted line in the figure). Fig. 1.6 thus demonstrates that the location of a magnetic-field-aligned boundary can be extracted whenever there is an intensity edge in an ENA image. The intensity can even vary along the edge without affecting the boundary identification. Simulations of TWINS images of the magnetopause (analogous to those shown in Figs. 1.3 and 1.4) indicate that the magnetopause can be extracted from Poisson statistics in 10-20keV H TWINS ENA images if a one-hour exposure is taken near apogee.

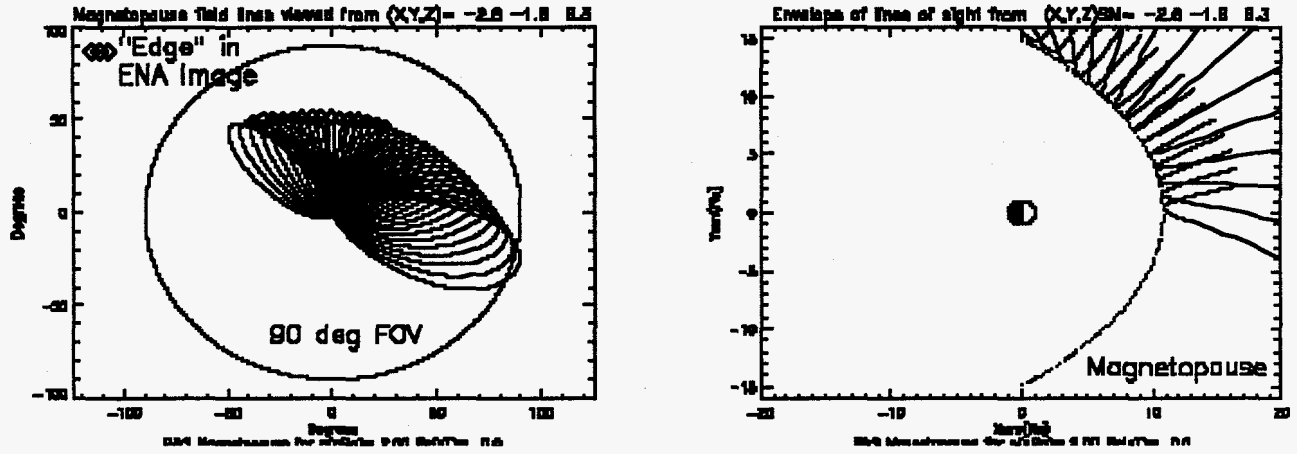

Figure 1.6 a) A "wire-model" of the dayside magnetopause viewed from near the post-midnight north polar cap in a Molniya orbit.. It is imagined that a trapped particle boundary (magnetopause) exists in the sector indicated by the diamonds, forming an intensity edge in an ENA image. b) Each LOS marked by a diamond along the edge in Fig. 1.6a is mapped into L-Φ coordinates. Their envelope clearly defines the

trapping boundary (magnetopause) that is indicated by the dotted curve, demonstrating a non-parametric algorithm for extracting particle boundaries from ENA images [Roelof, 1997].

With the stereo viewing from TWINS, the two views of the boundary may cover different regions of the boundary, they may overlap, or they may reveal two separate boundaries. Where they overlap, they provide a consistency check on the model used for the magnetic field. In any of these cases, the stereo views (as opposed to a view from a single spacecraft) will either greatly increase the precision of the extracted L-Φ dependence or will extend the range of the boundaries extracted.

1.2 Science Implementation

1.2.1 Instrumentation

For the TWINS mission, we have placed strong emphasis on maximizing the scientific return while minimizing the mission cost, risk, and development time. Our strategy to accomplish this goal is to utilize state-of-the-art instrumentation which we are currently developing for the IMAGE mission and to perform the minimum required modifications to accommodate the particular spacecraft. Specifically, TWINS will duplicate the instrumentation of the Medium Energy Neutral Atom (MENA) Imager on the IMAGE mission and adapt it to these mission of opportunity spacecraft.

The MENA imager design, and therefore the TWINS design, was chosen to provide high ENA sensitivity over a broad energy range. The primary technical issue for detecting and imaging neutral atoms in the space environment is that they must be measured against a large and ubiquitous UV background, which can produce high noise count rates in microchannel plate (MCP) detectors. To date, four different techniques have been developed to allow neutral atom detection and imaging against this background: 1) a thick foil which blocks the UV (viable energy range of 25-200 keV with a high geometric factor) [e.g., Mitchell et al., 1993], 2) an ultrathin charge conversion foil to ionize ENAs, which are than passed through an electrostatic energy analyzer (1-30 keV, moderate geometric factor) [McComas et al., 1991], 3) a charge exchange surface from which ENAs can reflect as ions which are then analyzed (0.05-0.2 keV, moderate geometric factor) [e.g., Wurz et al., 1995], and 4) transmission gratings which block UV but allow ENAs to pass (1-100 keV, high geometric factor) [e.g., McComas et al., 1997]. The TWINS science objectives require the combination of a broad ENA energy range covering the majority of magnetospheric plasma populations, a very high geometric factor, and high angular resolution. The transmission grating technique uniquely and fully meets all of these requirements. This technique has required significant advanced technology development during the MENA program to attain the extremely narrow grating dimensions that are necessary to sufficiently block UV. Further grating development will not be required for TWINS, eliminating the cost, time and risk associated with such development.

The sensor heads and the signal processing electronics of TWINS, including signal amplification, trajectory calculation, time-of-flight determination, and pulse height analysis, are identical to those of MENA, further reducing cost, risk, and development time. The primary differences between MENA and the TWINS imager are the DPU and the way the viewing plane is moved across the sky, both of which are spacecraft-driven. For IMAGE, the spacecraft spin will sweep the MENA field of view across the sky. Because the TWINS spacecraft are 3-axis stabilized, the sensor heads will be mounted on a rotatable actuator which sweeps the field of view over all pertinent look directions. The actuator will be nearly identical to one used for Cassini/CAPS. While the TWINS DPU and actuator are different from MENA, they have extensive heritage and do not add substantial cost, risk, or development to the TWINS mission.

The fundamental measurements made by a TWINS ENA imager are: (1) trajectory measurement of an ENA using the detected positions of the ENA and secondary electrons emitted as the ENA transits an ultrathin foil, (2) time of flight measurement between an ENA and its correlated secondary electrons, and (3) pulse height analysis of the detected signals. Imaging is derived from the trajectory measurement, speed is derived from the trajectory and time-of-flight measurements, and the ENA mass is inferred from the speed and pulse height analysis. The measurement technique schematic for each TWINS sensor head is shown in Fig. 1.7. Below, we follow an ENA through each sensor component:

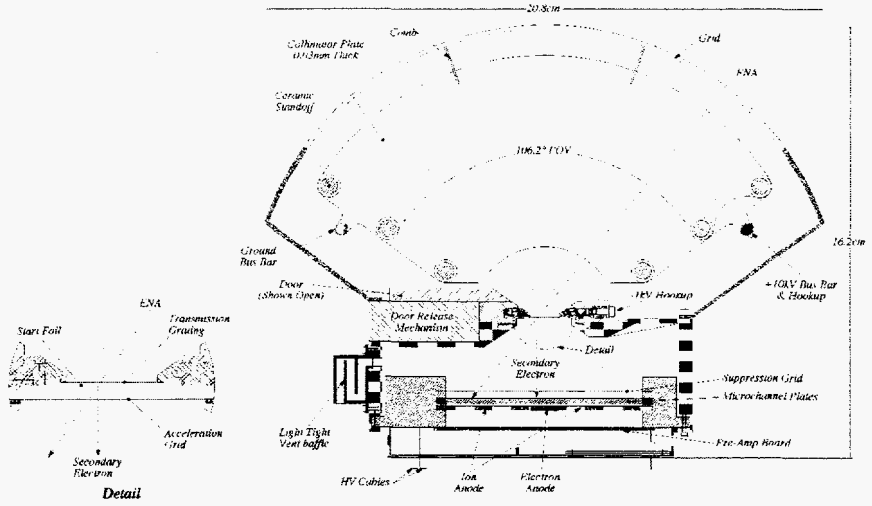

Figure 1.7 Schematic of a TWINS sensor head and the TWINS measurement technique.

Collimator Plates The collimator plates, which are identical to those of IMAGE/MENA, have a 2.7 cm inner radius and a 9.8 cm outer radius. The gap between adjacent plates is 0.5 cm. This geometry yields a 4° FWHM azimuthal field of view (FOV) and, with the plates alternately grounded and biased to +10 kV, rejects ions and electrons up to an energy of 130 keV/q, where q is the ion charge. The plates are blackened with a cupric oxide, highly dendritic coating that acts as an efficient absorber for UV photons, ions, and electrons.

Transmission Gratings The transmission gratings have been or will be used on the SOHO spectrophotometer SEM [Ogawa et al., 1993], the HETG spectrometer on AXAF [Schattenburg et al., 1994], and IMAGE/MENA. The gratings block UV by their waveguide properties while allowing ENAs to pass through into the sensor.

A freestanding transmission grating, illustrated in Fig. 1.8, consists of a series of gold bars, fabricated using holographic lithography, on top of a support grid. Considerable experimental and theoretical work has been performed to characterize the UV and ENA transmission properties of the gratings [Gruntman, 1995; 1997; Scime et al., 1995]. Fig. 1.9 shows experimental and theoretical results for a prototype grating 494 nm thick with a 200 nm period and an inter-bar gap of 62 nm [Gruntman, 1997; Funsten et al., 1997]. The experimental data (symbols) show excellent agreement with theoretical simulations (dashed line) for zeroth-order diffraction. The solid line, which is a theoretical result with all diffraction orders included, is representative of the grating performance for unpolarized light and follows a general exponential decrease of transmittance with increasing wavelength from 0.06 at 304 Å to 4×10^{-5} at 1216Å.

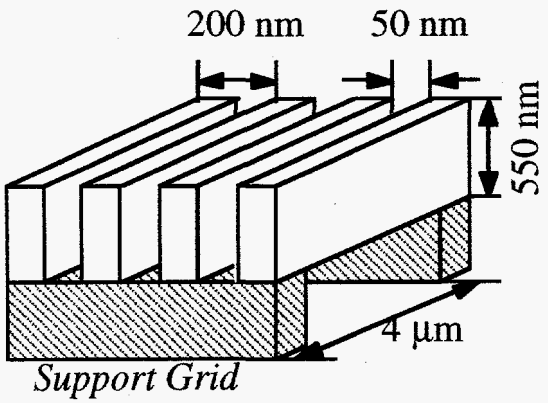

Figure 1.8 The TWINS flight-version transmission grating.

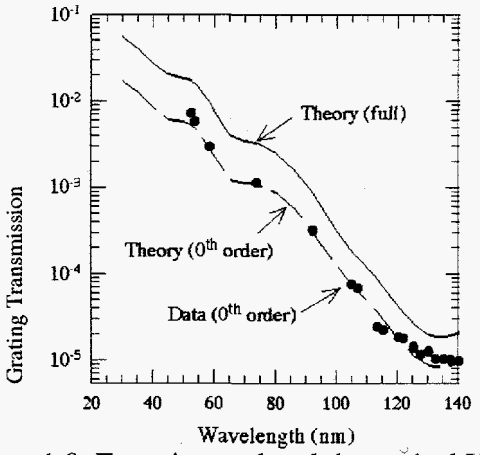

Figure 1.9 Experimental and theoretical UV transmission through a prototype grating.

The TWINS flight gratings have UV rejection properties which are significantly improved from this prototype grating. These improved gratings, which have been developed for IMAGE/MENA and will be delivered in the summer of 1997, have a bar width of 150 nm, a period of 200 nm, a gap width of 50 nm, and a thickness of approximately 550 nm. Theoretical results for this grating geometry, which should be extremely accurate based on previous results, predict ENA transmission of 12% and UV transmission of 5×10^{-7} at 1216Å.

Carbon Foil Immediately behind the transmission grating lies a nominal 50 Å thick carbon foil, which is mounted on a 333 line-per-inch, electroformed grid and is used to generate secondary electrons. These electrons produce the start pulse for a time-of-flight measurement of the ENA between the foil and the detector. Over an ENA energy range of 10-90 keV, the secondary electron yields have been measured to range from 2.1–4.5 for H, 2.3–5.8 for He, and 3–6.9 for O [Ritzau, 1997]. Identical foils are used on the Cassini Ion Mass Spectrometer (IMS) and will be used on IMAGE/MENA.

Angular scattering of projectiles in these foils is described by the equation $k_F = E\psi_{1/2}$, where k_F is a constant for a particular foil and projectile combination, E is the projectile energy, and $\psi_{1/2}$ is the angular scattering halfwidth at half maximum [Funsten et al., 1993; 1995]. For hydrogen, k_F = 13 keV-deg, giving $\psi_{1/2} = 3.4°$ at 4 keV and $\psi_{1/2} < 1°$ for $E > 13$ keV. This result shows that angular scattering in the foil slightly degrades ENA imaging resolution in the polar angle at energies less than 5 keV. Note that the azimuthal resolution is fixed by the collimator plates and is independent of foil scattering so that full image resolution is retained in this dimesion. In addition, energy loss of projectiles transiting these ultrathin foils is minimal [Funsten et al., 1995]. All TWINS flight foils will be fully characterized for thickness and pinhole content [Funsten et al., 1992a; 1992b].

While sputtering of the ultrathin foil due to ENAs and energetic plasma ions that transit the collimator is negligible [Funsten and Shappirio, 1997], sputtering of carbon by geocoronal oxygen can be quite high, with a sputter yield of 0.13 [Ngo et al., 1994]. Calculations show significant sputtering of the foil if it is exposed to RAM oxygen for 50 hours at 600 km altitude; this increases to 2,100 hours at 900 km altitude. Therefore, to maximize foil lifetime, the TWINS sensor heads will be covered by a reclosable door, which will be closed when the instrument points near the RAM direction at altitudes of less than 900 km.

Acceleration Grid The grating-foil assembly is biased to –1 kV. This bias sets up an electric field between the foil and the acceleration grid, which is located 1.5 mm behind the foil and is at ground potential. The field then accelerates secondary electrons directly downward to the detector. This acceleration enables the detected position of the secondary electrons on the detector to accurately represent the location at which the ENA transited the foil. The trajectory measurement is obtained using the detected positions of an ENA and its associated secondary electrons. The time-of-flight measurement is derived from the time difference between detection of the secondary electrons, which are detected first, and the ENA.

MCP Detector ENAs and associated secondary electrons strike a standard 10x10 cm microchannel plate (MCP) detector in a chevron (2-plate) configuration. An electric field, which is applied at the entrance surface of the MCP detector using a grounded suppression grid and a +100 V bias on the front of the MCP detector increases both the detection efficiency and the spatial resolution [Funsten et al., 1996]. TWINS will employ MCPs with a 60:1 length-to-diameter channel ratio. These MCPs are thicker and therefore mechanically more robust than conventional 40:1 MCPs, and produce a narrower pulse height distribution, which enhances identification of ENA species derived using pulse height analysis.

Detector Anode The ENA trajectory determination requires independent measurements of the one-dimensional (1-D) positions of the detected ENA and its associated secondary electrons. Furthermore, the time-of-flight (TOF) measurement requires independent measurements of the detection time of the secondary electron (start time) and that of the ENA (stop time). Therefore, the detector anode is segmented into two regions: the Start region, in which secondary electrons from the start foil are detected, and the Stop region, in which ENAs are detected. Each of these anode regions provides 1-D position encoding via a capacitive charge division technique and is serviced by two charge sensitive pre-amplifiers

(A and B). The relative pulse amplitudes on the A and B sides vary linearly with event position, allowing standard ratiometric position determination.

The system supports independent position determination on the Start and Stop anode regions to a full width spatial resolution of 1 mm, and TOF determination to a resolution of <20% for time ranges greater than approximately 7 ns, corresponding to the travel time of a 100 keV H atom at normal incidence. The independent position determination provides 1-D angular resolution of 3.8°, considering the 3 cm flight path between the Start foil and the MCP input face. The intrinsic energy resolution of the imager is $\Delta E/E = 2(\Delta t/t) = 0.4$, based on the 20% time resolution. The actual energy resolution can be set to any value larger than this, and since high spectral resolution is not as important as a high count rate for achieving the TWINS goals, we will choose an energy resolution of $\Delta E/E = 1$.

Pre-Amplifier Figure 1.10 shows a block diagram of the TWINS electronics. The pre-amplifier circuits are based on the Amptek A225 charge sensitive pre-amplifier. There are two pre-amplifiers (Start-A and Start-B) for the Start anode segment and two (Stop-A and Stop-B) for the Stop segment. For both the Start and Stop anodes, the A225 shaping amplifier outputs A and B are subjected to ratio analysis for position determination, while the fast A225 timing pulses are passed to the TOF card.

The Pulse Height Analysis (PHA) Card is used to determine the MCP pulse height and the 1D position of events on the Start and Stop anodes. The PHA Card has as inputs the shaped signals from the four pre-amplifiers. This card uses a peak and hold circuit to detect pulse peaks (via the zero cross on a first derivative signal), hold the level of the pulse peak, and disable further input until all signal processing for the current event is complete. The A & B signals are then fed to the inputs of a summing amplifier, and the sum is presented to the input of an A/D converter, which produces an 8-bit word representative of the MCP pulse amplitude. Additionally, the A signal (numerator) and the sum of A & B (denominator) are presented to a divider circuit, producing a ratio which is digitized to 8-bits. This 8-bit word is representative of the 1D position where the event occurred on the anode segment. This circuitry is implemented twice on the PHA card, to independently determine the pulse height and position of the event on the Start anode and on the Stop anode.

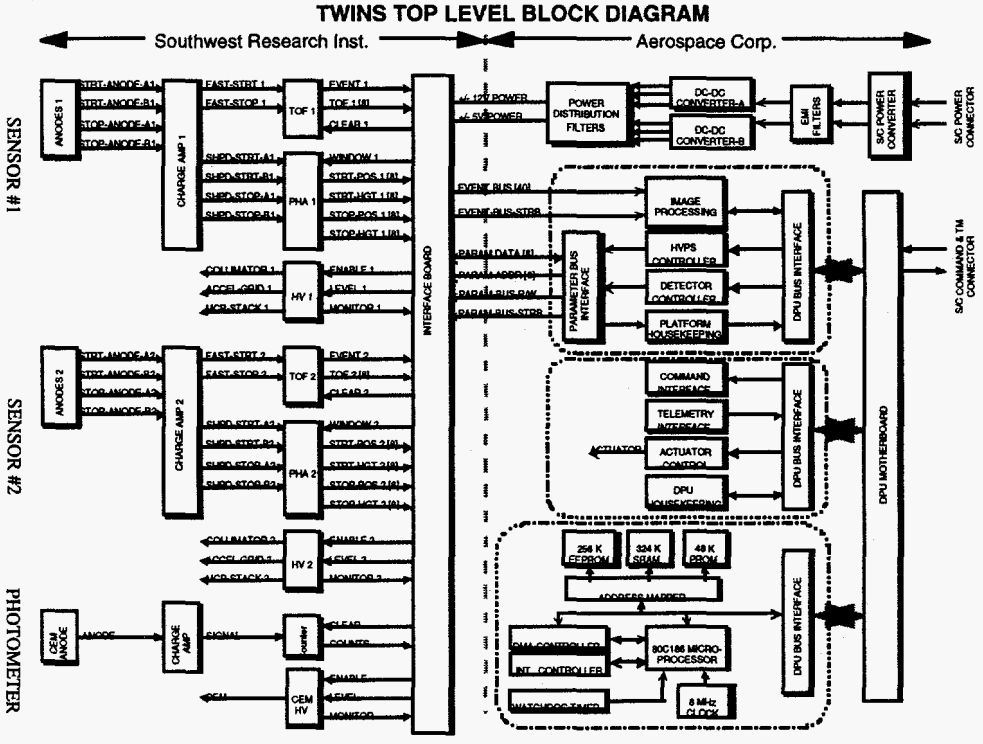

Figure 1.10 Block diagram of the TWINS electronics

The Time of Flight (TOF) Card is used to measure the time between Start and Stop for valid events. It uses the fast rising timing pulse outputs of the Amptek A225 charge amplifiers, which have not been processed with shaping filters. These fast rising pulses are fed into a constant fraction discriminator, which is used to control a time to amplitude converter. This amplitude is digitized and represents the time of flight of the primary ENA from the Start foil to the MCP input plane.

Lyman-α detector The Ly-α monitor is similar to the Hydrogen-Deuterium Absorption Cell (HDAC) Photometer that will fly on the Cassini mission. It utilizes a Ly-α notch filter constructed using an O_2 gas cell (high transmission for Ly-α, low transmission for most other wavelengths) with MgF_2 windows (low EUV transmission) and a KBr or CsI photocathode (low photoelectron yield for >180 nm wavelengths) on the channel electron multiplier (CEM). The monitor has four look directions, and the count rate from each monitor is measured every 1.33 sec, which corresponds to one pixel in azimuth on the ENA imagers.

HVPS The TWINS High Voltage Power Supply (HVPS) produces –1, +4, and +10 kV power on a single board. These provide the required HV bias to the carbon foil, the MCP stack and the Lyman-α , and the collimator plates, respectively. The instrument will use one such board for each sensor head, providing redundancy. The supplies are all switching supplies and can, if required, be synchronized. The topology used is resonant-flyback. This topology has been used on numerous instruments developed for flight or prototype, such as Cassini/CAPS, ELOP, MOSS, and DS1/PEPE.

Actuator To allow the TWINS instrument to view a range of azimuthal directions on these 3-axis stabilized spacecraft, each imager is located on a rotating actuator platform. The platform will rotate about the nadir direction (aligned with the center of the imager FOV) through a 360° range at a rate of 3° per second. This rotation rate, along with the symmetric orientation of the sensor heads, allows the entire field of view to be mapped out every 60 seconds (180°). The actuator has been used for Cassini/CAPS. It has a 4 year operational lifetime, and was designed to operate with minimal mechanical disturbances to the spacecraft. Control of the actuator platform will be provided by the DPU.

DPU The Data Processing Unit (DPU) uses flight-proven designs and high performance electronics to provide an intelligent and flexible control point for the TWINS instrumentation. Through the use of ground commands and stored command macros, the DPU software provides autonomous control of the TWINS sensors and a flexible means of allocating telemetry resources. The TWINS DPU is the same design as used for the Charged Particle Telescope (CPT) which has been recently qualified and delivered for launch this year on board an Air Force satellite.
CEM

The DPU is composed of a data section and a power section enclosed in a single chassis. The data section is comprised of three multilayer printed circuit boards (PCB): a CPU board, a spacecraft interface board, and a sensor interface board, which plug into a motherboard backplane. The CPU board uses an Intel 80C186 microprocessor. The data interface to the vehicle is accomplished through a MIL-STD-1553B bus interface protocol. Telemetry packetization and command reception and verification are performed by the spacecraft interface board through the use of a UTMC Summit 1553 protocol chip. The spacecraft interface board also provides control of the actuator and digitization of DPU housekeeping information such as temperature monitors, low and high voltage monitors, and current monitors. The sensor interface board provides data acquisition, image processing, high voltage control, and other sensor control functions. The power supply resides in a separate internal Faraday cage to minimize crosstalk between the DPU electronics and the power converters. The DPU supplies +5-volt power, ± 5-volt quiet analog power, and ±12-volt power to the TWINS instruments through two MDI DC/DC converter modules.

The DPU employs several risk mitigation techniques. It incorporates spaceflight quality radiation hardened components and latchup immune electronic devices. Single Event Upsets (SEU) are made nil through the use of voting logic in all gate array designs. Dual redundant and cross-strapped spacecraft interfaces minimize the risk of a spacecraft interface failure. The DPU has exceptional durability, achieved through the use of multilayer PCB technology and by minimizing internal harnessing through the use of right-angle PCB mounted connectors and a motherboard interface to all circuit cards. In-flight maintenance of the flight software, though not expected, is realizable through memory upload commands, and all memory can be examined through a special memory dump telemetry mode.

1.2.2 Instrument Performance

Based on the preceding description of the TWINS instrument, we now discuss the important features of the instrument performance, including TWINS data products, instrument viewing, sensitivity, and background count rates from UV. We demonstrate that the TWINS imager can be used to achieve the scientific goals of the TWINS mission. The full TWINS instrument specifications are listed in Table 1.1.

Table 1.1: TWINS Specifications

Parameter	Value	Comment
Geometric Factor	0.038 cm^2sr	Two heads
Polar FOV	+60 to -60° FWHM	Imaged
Polar Resolution [a]	4° FWHM	Imaged, Best case
Azimuthal FOV	± 2° FWHM	Collimated
Azimuthal Resolution	4° FWHM	Collimated
Energy Range	1-100 keV	TOF Window for H
Mass Identification	H, O	TOF + PHD
Energy Resolution, (ΔE/E) [b]	0.4	TOF + mass
Time Resolution	60 sec	Actuator rotation period
UV Rejection	$4.7x10^{-9}$	Worst Case

[a] Mass and energy dependent. Angular resolution is slightly degraded in one dimension for H atoms with $E < 5$ keV and O with $E < 40$ keV.

[b] Speed measured by TOF and trajectory; energy inferred from species identification and speed.

Data Products The telemetry allocated to the TWINS instrument is 4 kbps. One data histogram will be telemetered every 60 sec (the actuator 180° rotation time), so 240 kb are available at each time step. The basic data product consists of an image formed by the number of counts in each pixel for a given velocity and time interval. Excess bits are used for data from the Lyman-α detector; for singles data, consisting of raw position, time-of-flight, and pulse height data for a sample of valid single events; and for housekeeping and diagnostic data. Data from each sensor are independently telemetered so response variations between the two sensor heads can be identified and applied to subsequent analysis. Sample one-minute histograms, representing trade-offs between spatial and speed or mass resolution are shown below. Higher speed and mass resolution could also be achieved by integrating for a longer time interval.

- High spatial, low speed resolution histogram: 24 polar bins (96° FOV/4°) x 45 azimuth bins (180°FOV/4°) x 2 sensors x [7 speed + 3 mass bins] x 10 bits (compressed) = 216 kb

- Low spatial, high speed resolution histograms: 16 polar bins x 30 azimuthal bins x 2 sensors x [24 speed, pulse height, and/or mass bins] x 10 bits (compressed) = 230 kb

- Singles data: 8 bit start + 6 bit stop + 8 bit TOF + 6 bit PHA start + 6 bit PHA stop = 34 bits

- Lyman-α data: 4 pixels x 45 aximuth bins (180°/4°) x 10 bits (compressed) = 1.8 kb

Field of View As indicated above, the collimator plates restrict the azimuthal field of view to 4°. The intrinsic polar angle resolution is also 4°. Figure 1.11 shows the calculated polar angle response of each of the imager heads (red and green lines). The response of each head is appreciable over a range of approximately ±45° from the normal, except for a notch near 0°. This notch is due to the presence of the secondary electron anode, which lies directly below the grating and replaces that portion of the ENA anode.

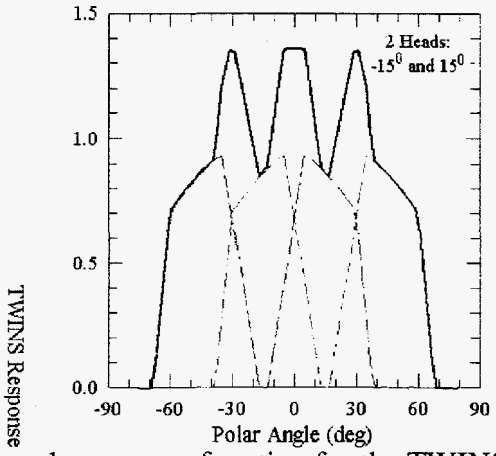

Figure 1.11 The polar angle response function for the TWINS sensor heads at +15° (green) and –15°(red), and for the total two-headed instrument (black).

Each TWINS instrument will carry two sensor heads, mounted on a scan platform whose normal points in the Earth nadir direction. The normals to the detector planes of the two heads will be cocked at polar angles of +15° and –15° relative to the nadir. With a ±45° field of view for each head, the two heads together will thus cover a polar angle range from –60° to +60° FWHM, with a 60° overlap in viewing centered on the nadir direction. In the region of overlap, the notch in the response function of one head is filled by a response peak of the other head (black line in Fig. 1.11). Thus, between the two heads, there is full coverage of the viewing cone within each 180° scan. In a full 360° scan, each pixel will be sampled twice, once by each head, allowing cross-calibration, consistency checks, and some back-up redundancy.

From a radial distance of 7 (5) R_E, the TWINS field of view extends to 12.1 (8.7) R_E from the Earth in the plane perpendicular to the nadir vector. The corresponding intrinsic spatial resolution for the ENA imager (with 4° angular resolution) is 0.49 (0.35) R_E. Even with some smearing due to the motion of the scan plane, this coverage and resolution are quite adequate to monitor the global evolution of boundaries and injection fronts.

Sensitivity The full TWINS instrument geometric factor with two sensor heads is calculated in Table 1.2. The geometric factor is the product of: 1) the ENA transmission rate (see Table 1.3), 2) the sensor FOV, 3) the sensor aperture area, 4) the response function of a sensor head (Figure 1.11), and 5) the probability of secondary electron emission at the foil, since both an ENA and its associated secondary electrons must be detected for a valid measurement. The total geometric factor for the two-headed instrument is 0.038 cm^2sr. This value reflects the large aperture area of a grating-based imager. The average geometric factor for a 4°x4° pixel is $G_p \approx 1.4x10^{-3}$ cm^2 sr, based on a 120° field of view for the two-headed instrument.

Table 1.2: Geometric Factor

ENA Transmission	0.036
Secondary electron emission probability at foil (10 keV H)	0.85
Azimuthal FOV	+/- 2° FWHM
Polar FOV (single head)	+/- 48° FWHM
Response Function Average (per head)	0.6
Aperture Area (single head)	8.6 cm^2
Single Head: G_1 = 0.036*0.85*0.12 sr*0.6*8.6 cm^2 = 0.019 cm^2sr	
Two Heads: $G_2 = 2G_1 =$ **0.038 cm^2sr**	
Per Pixel: $G_p = G_2/30 = 1.4 \times 10^{-3}$ cm^2sr	

The imager sensitivity, or the number of ENA counts (C) obtained in each pixel over each camera scan is

$$C(\text{counts/pixel/scan}) = D\,\Delta t\,G_P\,\Delta E\,j_{ENA} \qquad (1.2)$$

where D is the duty cycle (fraction of a scan that a point in the sky is viewed by the detector through the collimator), Δt is the scan time, G_p=1.4x10^{-3} cm^{2}sr/pixel is the instrument geometric factor per pixel, and j_{ENA} is the ENA intensity given by Eq. 1.1. From Eq 1.1, we define a new integral, $I_{ENA} = j_{ENA}/(\sigma R_E j_{ion}^{max})$, which has units (cm^{-3}); it depends only on the geocoronal density and the morphology of the ion distribution (now normalized by j_{ion}^{max}, the maximum ion intensity occurring in the magnetosphere). Introducing these relations into Eq. 1.2 we find that the counts/pixel/scan are

$$C = D\,\Delta t\,G_p\,\Delta E\,\sigma\,(6.37\text{x}10^8\text{ cm})\,j_{ion}^{max}\,I_{ENA} \qquad (1.3)$$

where for 10 keV protons, σ=7.75x10^{-16}cm^2, and ΔE=10 keV. The nominal duty cycle per pixel is D_0 = 4°/180° = 0.022. At polar angles near nadir, a given point in the sky can be viewed between the collimator plates for a large fraction of the 180° scan, resulting in an effectively larger duty cycle D(θ) for viewing near the nadir direction. The pixel centered at 0° polar angle has essentially a 100% duty cycle. For parallel collimator plates with a 4° acceptance angle, the duty cycle can be shown to be $D(\theta) = (2/\pi)\sin^{-1}(\tan(2°)/\sin\theta)$ for θ>2° and D(θ)=1 for $\theta\leq$2°. Bearing in mind then that $D(\theta)/D_0$ can be as large as 45 for near-axial pixels, and using the TWINS instrument parameters given above, Eq. 1.3 yields

$$C(\text{counts/pixel/scan}) = (9.1\text{x}10^{-9})\,(D/D_0)\,j_{ion}^{max}\,I_{ENA} \qquad (1.4)$$

for a 180° (60 second) scan, where j_{ion}^{max} has units of (cm^2 s sr keV)$^{-1}$.

Eq. 1.4 suggests a very useful plot (Figure 1.12) for the display of the sensitivity of the TWINS cameras: a contour plot of C as a function of $\log_{10}I_{ENA}$ and $\log_{10}j_{ion}^{max}$. In this figure, we have assumed a duty cycle $D(\theta)/D_0$ = 2.9 (θ = 20°) representative of near nadir viewing. For empirically based models of ring current and ion injection events, the maximum value of I_{ENA} is of the order 10^4 cm^{-3} while observed maximum intensities of energetic ions (e.g., protons 1-30 keV) in large magnetic storms are in the order of j_{ion}^{max} >10^6 (cm^2 s sr keV)$^{-1}$ at geosynchronous orbit. The top edge of the plot represents the brightest pixel in the image (usually on night-side sub-auroral field lines at low altitudes where the hydrogen geocoronal density is the highest), while the lower edge represents the outer region of the pre-noon trapping region, where the energetic ion intensities are lowest. The left edge of the plot corresponds to

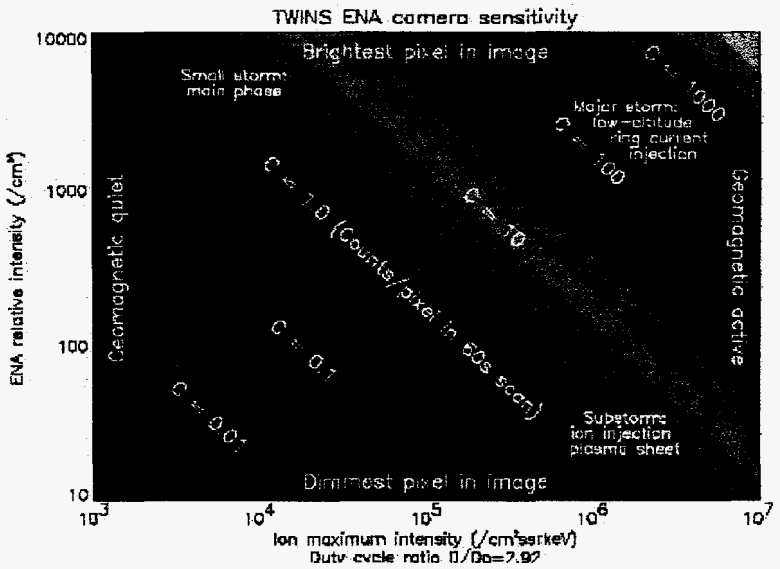

Figure 1.12 The sensitivity of a TWINS imager in counts per pixel in a 60 second (180°) scan. The horizontal axis shows maximum ion intensity during an image, and the vertical axis shows the ENA brightness across that image.

11/18/97nearly quiet geomagnetic conditions, and the right edge to major disturbances (e.g., ring current during storm main phase, active substorm ion injection events). The fact that C>100 counts/pixel/scan in the upper right corner verifies that TWINS can obtain 10% Poisson statistics in the brightest 4°x4° pixels in a major storm with 1-minute time resolution. Averaging in time will allow us to obtain good statistics for weaker events. At the C=1 contour level, if counts are summed over four adjacent 4°x4° pixels, 10% statistics can be achieved with a one-half hour exposure. This is sufficient to characterize the brightest low-altitude emission in the main phase of a small storm (j_{ion}^{max}~10^3), an ion heating event in the near-Earth plasma sheet, or the outer regions of the trapped energetic protons (e.g., the magnetopause "edge" in Fig. 1.6) during the main phase of a major storm (j_{ion}^{max}~10^6).

The image unfolding procedure discussed in Section 1.1.4 requires energy and mass identification of the detected ENAs. In the TWINS instrument, mass identification is based on pulse height analysis. This instrument can distinguish H from O, but He is not well resolved. The mass resolution technique is essentially the same as that being used for the Cassini INCA instrument [Mitchell et al., 1993], and for HENA and MENA on IMAGE.

UV Background Table 1.3 compares the UV transmission and ENA transmission for the full instrument, including all components of a sensor head. Fig. 1.13 shows the dayglow UV flux at solar minimum as a function of wavelength both before and after the transmission grating, for the prototype grating discussed above. Although the grating is less efficient at blocking UV at shorter wavelengths, the geocoronal flux at these wavelengths is far less than at 1216 Å. The integrated dayglow flux is $5.5x10^4$ R [Meier, 1991] and the total flux transmitted through the prototype grating is 14 R (from Figure 1.13). Based on the instrument geometry factor and the UV transmission rate (Table 1.3), this corresponds to a sensor count rate of ~10^2 cts/sec. Assuming a time-of-flight window of 100 ns and count rates of 8000 cts/sec and 2000 cts/sec on the ENA and secondary electron anodes, respectively, the coincidence rate due to UV is 1.6 events/sec.

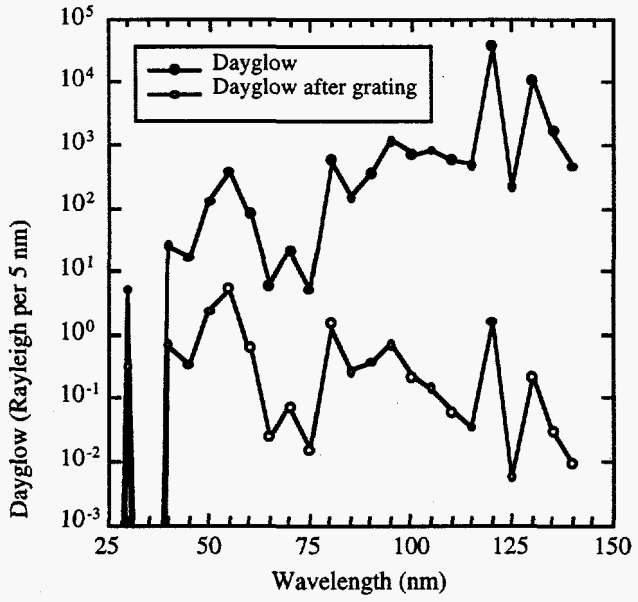

Figure 1.13 Dayglow UV flux, before (solid) and after (open) a prototype transmission grating.

Two factors will result in an actual background count rate less than this value. First, this calculation assumes that the UV is incident normal to the gratings. The equivalent grating thickness increases with increasing polar angle, and the transmission exponentially decreases for these higher polar angles of incidence. Second, the MENA and TWINS flight gratings (which are already developed and will be delivered this summer) will be thicker and have a narrower gap than the prototype grating, resulting in a further reduction in UV transmission by a factor of almost 100, giving total UV transmission at 1216 Å of $4.7x10^{-9}$ for the flight gratings. This corresponds to an integrated UV background coincidence rate of 0.02 events/sec, or 1.2 counts in 60 seconds (approximately 0.04 counts per ENA pixel). For the

geophysical phenomena of interest (see Figure 1.12), UV will thus not introduce significant noise in the ENA measurements.

Table 1.3: UV and ENA Transmission and Detection

Part	UV (1216 Å) Transmission	ENA Transmission	Technique
Grating: - Prototype - MENA and TWINS	 $4x10^{-5}$ $5x10^{-7}$	 0.12 0.12	 measured calculated
Foil	0.4	1	measured
Grids: - collimator - Foil mount - Acceleration - SE Suppression	 0.9 0.65 0.9 0.9	 0.9 0.65 0.9 0.9	 vendor spec. measured vendor spec. vendor spec.
MCP sensitivity	0.05	0.9 (ions) 0.7 (electrons)	measured estimated
Total: - Prototype - MENA and TWINS	 $3.8x10^{-7}$ $4.7x10^{-9}$	 0.036 0.036	

In this section, we have shown that the TWINS imager is able to make measurements which will allow us to achieve the scientific goals of the TWINS mission. The instrument sensitivity, energy, time and angular resolution, and field of view will enable viewing of the magnetosphere out to a distance of 10-12 R_E and identification of the structure of the magnetosphere, including the identification of different regions and boundaries. We will be able to image the magnetosphere with a time resolution of a few minutes for both active and quiet conditions (Fig. 1.12), and thus will be able to observe the evolution of the magnetosphere through various levels of activity. The imager has sufficient energy, mass, and angular resolution to allow observation of the details of the plasma populations in different regions of the magnetosphere, including the motion and energization of particles between different regions. The stereo viewing capability of the two TWINS spacecraft will reduce our dependence on models, allowing a quantitative unfolding of ENA images and providing for the first time a picture of the 3D structure and evolution of the magnetosphere.

1.2.3 Mission

The ideal orbit for a magnetospheric imaging mission is one in which the spacecraft spends a large fraction of the time at relatively high altitudes (> 5 R_E) and high inclination angles (> 60°) so the imager can view the equatorial magnetosphere out to a distance of many Earth radii. From this viewing angle, the imager can simultaneously image different regions of the magnetosphere, allowing the evolution of and particle motions between different regions to be clearly observed. The Molniya orbit of these mission-of-opportunity spacecraft is ideal for this purpose, since it has a high altitude (7.2 R_E), a high inclination angle (63.4°), and the majority of the orbit period is spent near apogee.

It is also desirable that the imager spend much of the time pointed towards the region around the Earth, since obviously the magnetosphere can only be observed with these look directions. The TWINS spacecraft are approximately nadir pointing (within 25°), which means that the TWINS instruments will directly observe the magnetosphere throughout the mission.

A third criterion is that the imager be able to view a large range of directions, in order to observe asymmetries in the magnetosphere. Since the spacecraft for this mission are 3-axis stabilized, this range is achieved on TWINS with a rotating actuator platform, which allows the entire viewing cone to be mapped out on a 1 minute time scale. In short, the spacecraft orbits for this mission of opportunity are almost

exactly those that would have been selected for an independent magnetospheric imaging mission, and are ideal for achieving the stereo viewing goals of the TWINS mission.

1.2.4 Data Analysis and Archiving

The TWINS team is committed to making the data from this mission available to the entire scientific community and to the general public as quickly as possible. The team will need to validate the data and produce higher level products to make the data useful for scientific and educational purposes, but claims no special or proprietary rights to the data. Our Education and Outreach plan goes well beyond simply making TWINS data available to the public. Rather we intend to communicate both TWINS results and the excitement of being able to visualize the 3-D structure and dynamics of the near-Earth space environs to the public for the first time.

For this mission of opportunity, the spacecraft sponsor will provide data telemetry and recording of data on the ground. The sponsor will extract the TWINS science data from the raw telemetry stream and forward these data packets to the Aerospace Corporation. Aerospace, under the direction of Co-I Dr. B. Blake, will be responsible for organizing these raw data by viewing direction and forwarding this data product to LANL for subsequent processing. This processing will map instrument counts onto geomagnetic and geographic coordinate systems so that images may be easily compared to each other and to previous and complementary data sets.

We will process the TWINS Level 0 data as it becomes available. The entire Level 1 data set and higher level data products will then be available through a host server which can be readily accessed by the TWINS science team members and the relevant data downloaded to the team member's institution immediately. Data at this level will also be made available to other scientists. The team will also produce higher level data products, including images as a function of energy and species from each of the spacecraft, and stereo images from the combined two spacecraft measurements.

All data will be archived at LANL as soon after processing and validation as possible. This time frame will range from hours to months depending on the complexity of the specific data product. The basic data unit for TWINS consists of 1-minute histograms of instrument counts as a function of azimuth, polar angle, velocity and mass. Both raw, validated data and histograms corrected for instrument response will be archived. Lyman-α data, consisting of counts as a function of look direction, will also be archived. In addition, we will archive higher level data products, including both single spacecraft and stereo images. The format for these submissions will be standardized for easy access and use by the TWINS team and by other researchers. We also plan to provide TWINS data to the National Space Science Data Center (NSSDC) to facilitate dissemination to the scientific community.

The TWINS science team has specific and detailed research objectives in mind. This analysis typically requires the full data sets from both TWINS sensors. The interpretation and science extraction activities will be multifaceted. A first level of interpretation will involve the 3-D visualization of the structures and evolution of the imaged regions, and the examination of temporal and spatial correlations between the different regions. Major controversies may be resolved by this level of analysis alone. We will involve other data sets that are available in these analyses, including geosynchronous and low altitude in situ measurements and measurements made from the ground. Quantitative parameter extraction will be done using various levels of image unfolding or "inversion" techniques (Section 1.1.4) that our team has pioneered for the magnetospheric imaging problem. Such quantitative information will allow us to attack the problems of global electrodynamics for some regions. Finally, careful comparisons will be made between the evolving images and predictions based on first principle simulations. For example, image predictions based on both MHD and large-scale kinetic models were shown in Section 1.1.4. These comparisons will be used to guide the modification of the physical models. Our team has substantial expertise in these areas, and it is our expectation that a much broader modeling community will involve themselves in this process once the images become available.

The TWINS team plans a hierarchy of analysis methods and products to assure that TWINS results are available to the interested citizen, to scientists requiring solar-terrestrial global images for context, and to

other scientists performing detailed scientific analysis. Our education and outreach plan is summarized in Section 2.1. The TWINS team will share these new images of the Earth's plasmas and upper atmosphere with the public. Rapid and frequent public access to the TWINS stereo images will be facilitated with software and displays that will allow the creation of easily-understood images and movies from the TWINS data set. We expect that the TWINS data will enable new approaches for researchers working on other magnetospheric and ionospheric problems. Thus, in addition to the on-line images (which will have scientific value as well as public appeal), we will also provide more quantitative and detailed analysis results as rapidly as possible so that space scientists can readily ascertain the state of the solar wind-magnetosphere-ionosphere system. Access will be via the TWINS internet home page at LANL.

1.2.5 Science Team

The TWINS Science Team consists of the Co-Investigators and related personnel at the Co-I institutions for this mission. They bring a unique blend of expertise in mission management, neutral atom imaging hardware (INCA/Cassini, MENA/IMAGE, and HENA/IMAGE), magnetospheric physics (data analysis from geosynchronous satellites, POLAR, etc.), and image deconvolution techniques and algorithms. Table 1.4 gives the primary scientific responsibilities of each institution. Appendix 1 gives detailed resumes and specific areas of expertise for each of the Co-Investigators.

Table 1.4: Scientific responsibilities of Co-I institutions.

Institution	Responsibilities	Investigators
LANL	L0 and L1 data processing Data validation Data archiving Outreach	D. McComas H. Funsten R. Skoug
Aerospace	Contact with Sponsor Preliminary data processing	B. Blake
SwRI	L0 and L1 data processing software	J. Burch C. Pollock
APL	Image inversion techniques	E. Roelof D. Mitchell
USC	Image inversion	M. Gruntman
WVU	L0 and L1 software	E. Scime

2.0 EDUCATION, OUTREACH, TECHNOLOGY, AND SMALL DISADVANTAGED BUSINESS PLAN

2.1 Education and Outreach Plan

By providing the first stereo views of the Earth's magnetosphere, TWINS images will not only introduce a new avenue of magnetospheric and plasma space science, but will also excite the general public, science educators, and students with their dramatic portrayal through pictures of the structure and dynamics of the Earth's plasma environment. Through the TWINS images, magnetospheric physics will be able to join astrophysics in the ability to convey the thrill of discovery in vivid pictures in the news and education media. TWINS images, like those simulated in this proposal, will captivate the public as we explore the outer reaches of the Earth.

The TWINS team is committed to a full and vigorous Education and Outreach program. The outreach program, which will be managed from LANL, will include a Co-Investigator from each institution, who will coordinate outreach activities in their region. The team members will be: Dr. R. Skoug (LANL), Dr. C. Pollock (SwRI), Dr. M. Gruntman (USC), Dr. E. Scime (WVU), Dr. B. Blake (Aerospace), and Dr. E. Roelof (APL).

Our outreach program will be based on guidelines outlined in recent documents on national education, such as the NASA "Partners in Education" [1995] and the AAAS "Benchmarks" [1995] documents. The goals outlined in these documents include a strengthening of interest in science and exploration, as well as the development of science thinking skills and teaching of basic science concepts that cut across and unite the fields of science: energy, patterns of change, stability, systems and interactions, and scale and structure. Recommendations include developing partnerships with educational institutions and developing a wide range of educational tools to reach a diverse audience of the public and students. Our outreach plan will focus on these same guidelines: We will reach students through partnerships with teachers and national educational associations, and the development with them of educational materials. We will address a broader audience through partnerships with museums, through a World Wide Web page, and by disseminating TWINS results through the news media. We offer here a few examples of the creative approach we intend to follow in getting TWINS scientific results and space physics concepts in general to a broad audience.

A first step in our outreach program will be to develop tools for viewing the 3D images produced by the TWINS imagers. This effort will include the development of a stereo viewer and the combination of images into movies that show changes of the plasma with time. Tools of this type will be suitable for inclusion in museum displays and classroom demonstrations, and we will strive to reach a broad audience with these displays.

We will work directly with teachers to develop educational tools which can be used in the classroom to teach science in general and space science in particular to students at various levels. Such tools may include hands-on classroom experiments, software lessons, and a World Wide Web page devoted to science education. We will endeavor to create a range of tools in order to reach a diverse audience. This outreach will be coordinated through the Los Alamos Science Education Group to take advantage of their experience in curriculum development and in conducting workshops for teachers and students.

Further, we will create a summer internship program for high school students, in which students will spend several weeks at a TWINS institution and participate in the analysis of TWINS data. The benefits of this program will be two-fold. The high school students will develop an understanding of scientific research through work with the TWINS image data. In addition, upon return to their home schools, they can share what they have learned about space science with their peers and with younger students in their communities.

To reach the general public, TWINS results will be distributed through press releases to newspapers and TV stations, and will be displayed on a TWINS World Wide Web page run at LANL. Again, the movie format most suitable for viewing the images is also well suited to a television display.

Through its various Co-I institutions, the TWINS team has strong connections with a wide variety of educational institutions, listed in Table 2.1. We will tap into existing educational programs at TWINS team member institutions that provide teacher training and curriculum development and can assist with the identification of students for internship programs. The team has connections with a number of museums where TWINS images can be displayed. In addition, since our data products are related to those produced by the NASA IMAGE mission, we will be able to work with the IMAGE Education and Outreach team and to extend their programs both through the inclusion of new data and through expanding their audience to include new institutions.

From educational strategies to media strategies, TWINS images will open a window on space physics into the national consciousness. To share the excitement these images will generate with the public, we have proposed a vigorous Education and Outreach program which is imaginative, but is solidly grounded in basic education concepts, connections with existing educational organizations, and diverse communications channels.

Table 2.1. TWINS Education and Outreach Connections

NASA	Teacher Resource Center Network Regional Teacher Resource Centers Space Grant Consortia Classroom of the Future
SWRI	NASA IMAGE Mission Outreach program Young Scientist and Engineers (YES) program
USC	Educational Television Channel Instructional Television Network California Museum of Science and Industry
WVU	Wheeler Jesuit College -- NASA Classroom of the Future Maryland Science Center
LANL	Science Education Group University Outreach Team Community Involvement and Outreach Office Bradbury Science Museum
AGU	American Geophysical Union
AIP	American Institute of Physics
AAAS	American Association for the Advancement of Science
NSTA	National Science Teachers Association
AIAA	American Institute of Astronautics and Aeronautics

2.2 Technology

The strategy for the TWINS mission is to use existing instrument designs for the TWINS imager. One new technology is used for the TWINS instrument: The transmission grating used to block UV represent a significant increase in technology. These gratings were developed for IMAGE/MENA, and will first be flown on the IMAGE mission. TWINS is thus able to take advantage of this state-of-the-art grating technology without incurring the costs or risks associated with the development process.

2.3 Small Disadvantaged Business Plan

The TWINS team will substantially involve Small and Small Disadvantaged Businesses in meaningful roles throughout the program. LANL has estimated $200,000 in machine shop work to be purchased from local vendors, all of which qualify as small, minority-owned businesses. This amounts to over 9% of the LANL Phase B/C/D cost estimate. Similarly, the other hardware institutions, SwRI and Aerospace, have identified machine shop and circuit board fabrication work to be performed by SDBs amounting to approximately 9% of their Phase B/C/D costs. In Phase E, TWINS team institutions plan to involve SDBs in data system purchase, set up, maintenance, and operation.

As the Lead Institution, LANL will direct and help team members identify areas of SDB involvement at each major institution. We will also lead an effort, if necessary, to locate qualified SDBs to match the tasks, using Internet news groups, the Thomas Register, other communication media, and the LANL Industrial Partnership Office. Obvious areas for SDB involvement include CADCAM operators, mechanical and electrical design engineers and consultants, printed circuit board fabrication and assembly vendors, test laboratories, software engineers, and data acquisition technicians. SDB involvement in all these areas have been used in the past by one or more of the TWINS team institutions

The search for qualified SBs and SDBs will continue through all phases of the TWINS program. The PI and PM will be kept informed of progress made in awarding subcontracts and purchase requests to small businesses. We will maintain a record of awards made to small disadvantaged businesses and report our efforts in this area to NASA's small business advocate.

3.0 MISSION IMPLEMENTATION

3.1 Mission Design

For this Mission of Opportunity, we have been invited to participate in missions on two identical United States spacecraft, referred to in this proposal as S/C-1 and S/C-2. The host spacecraft will carry particle instrumentation for making scientific and space weather measurements, consisting of an energetic particle spectrometer/dosimeter and a plasma analyzer. These instruments are improved versions of two currently flying and one to be launched on similar host spacecraft. The plasma analyzer measures the fluxes and spectra of electrons and ions from 50 eV – 30 keV using standard electrostatic analyzer techniques. The spectrometer/dosimeter covers the electron energy range from 50 keV to >5 MeV and the proton energy range from 70 keV to >80 MeV. A direct measurement also is made of the dose in Rads(Si) under 5 aluminum shielding thicknesses. The data from these instruments were first used for space weather purposes, and now scientific uses have begun [Blake, 1990; Blake et al., 1997; Fennell et al., 1997; Grande et al., 1997]. Several studies are underway using these data in concert with POLAR and SAMPEX observations. In addition, the data from the current instruments are used routinely for space weather purposes by the host program and Air Force space weather personnel. The energetic particle instrumentation aboard the TWINS missions will provide important support for the TWINS investigation by indicating the presence and the intensities of energetic particles in the local spacecraft environment.

Each host spacecraft will be placed in a Molniya orbit with an inclination angle of 63.4°, a perigee altitude of several hundred kilometers, and an apogee in the northern hemisphere at an altitude of 7.2 R_E. The specific inclination of 63.4° is used because it results in an orbit with a fixed argument of perigee. The semi-major axis is such that the spacecraft has a period of one half of a sidereal day, giving fixed longitudes of apogee. The local time of apogee moves through 24 hours every 326 days. The Atlantic apogee of the spacecraft is specified to be within 40 degrees West to 20 degrees East. The orbit of these host spacecraft are thus similar to that optimized for magnetospheric imaging on the IMAGE mission. The spacecraft are 3-axis stabilized, and are approximately nadir pointing. These nadir pointing spacecraft are ideal for the TWINS scientific goals, since the imagers will rotate about an axis pointed towards the Earth at all times and thus will always observe the magnetosphere.

The first of these satellites (S/C-1) will be launched in late 2001 or early 2002, with the second (S/C-2) launched approximately two years later. The launch vehicles and integration of the scientific instruments to the spacecraft will be provided by the mission sponsor. The precise launch dates are not known, and so we have used the delivery dates to the sponsor for developing the schedule outlined in this proposal. The design lifetime for each spacecraft is approximately 7 years, but the TWINS imagers will be designed with a nominal lifetime of 4 years. This represents a doubling of the design lifetime of the IMAGE/MENA imager, which is easily achievable through selective radiation shielding of the most sensitive components. In addition, the TWINS mission takes place further from solar maximum than the IMAGE mission, and thus TWINS will encounter a more benign radiation environment. The TWINS time scale provides stereo viewing during a two-year window of simultaneous observations by the imagers on the two spacecraft. Depending on the exact launch date, we may also achieve simultaneous viewing time with the IMAGE spacecraft, to be launched in 2000.

3.2 Instrument Accommodation

A detailed list of the spacecraft resources required for the TWINS instrument is given in Table 3.1. The total mass of the scientific instruments is approximately 13.6 kg, the total power consumption is 15 W, and the data rate will be 4 kbps. The scientific instruments will be located on a platform on the bottom of the spacecraft, nominally pointing in the nadir direction. The dimensions of the platform are 57 x 57 cm, and the instruments extend outward from the platform by a distance of 30 cm. Figure 3.1 shows a sketch of the instrument layout on the platform. Since the spacecraft is 3-axis stabilized, the sensors will be located on an actuator platform to allow viewing in different directions. The actuator rotates through 360°

in a windshield-wiper motion with a rotation speed of approximately 3° per second. Since the two heads are symmetrically oriented about the nadir direction, the full distribution is mapped out every 60 seconds.

TABLE 3.1: Instrument Resources

Mass	13.6 kg
Power	15.0 W
Footprint	57 x 57 x 30 cm
FOV	± 60°
Commands	1 16-bit word
TM Rate	4 kbps

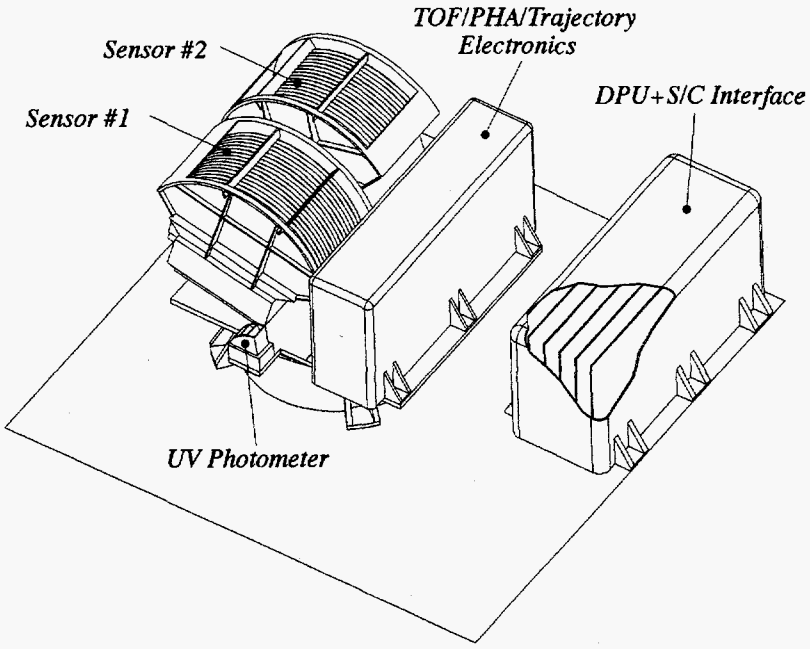

Figure 3.1 Layout of the TWINS instrument on the spacecraft scientific instrument platform.

Power and telemetry for the TWINS instruments will be provided by the spacecraft. The single-point interface to the spacecraft will be through the instrument DPU. This box will provide power regulation and formatting of the data signal to be sent to the spacecraft telemetry system. Data telemetry, recording of data on the ground, and preliminary data processing to extract the scientific data will be provided by the sponsor. The scientific data will be sent to the TWINS team for further processing and validation. Uplink command capability will also be available through the sponsor.

3.3 Potential Risk Areas

One of the strengths of this proposal is that it draws heavily on existing technologies and the MENA instrument design. In addition to reducing mission costs and development time, this strong heritage greatly reduces the potential risk involved in this mission.

One potential risk area for any instrument is the possibility of a high voltage power supply failure. This risk is mitigated through the use of independent power supplies. Each sensor head has separate high voltage supplies for the collimator voltage and the MCP voltage. A failure of one high voltage supply would thus affect only one of the sensor heads. This loss of one sensor head would lead to a reduction in geometric factor and in field of view, but would not terminate the TWINS mission.

4.0 MANAGEMENT AND SCHEDULE

Management of the TWINS investigation will be the responsibility of LANL. All portions of the two identical instruments will be integrated, tested, and fully calibrated at LANL and will then be turned over to Aerospace for final delivery to the spacecraft sponsor. Our approach to management of the TWINS program is based on decades of experience at LANL in successfully leading space instrument projects, including instruments on IMP, ISEE, Ulysses, Lunar Prospector, ACE, and numerous other programmatic missions.

4.1 Project Organization

TWINS is organized around two existing and successful working relationships and has only three institutions involved in the instrument hardware development and delivery. In addition to close collaboration on Cassini/IMS and DS-1/PEPE, LANL and SwRI are presently jointly developing the IMAGE/MENA instrument which is the basis for TWINS. This relationship will be maintained for TWINS, and these two institutions will build the bulk of the proposed hardware. The Aerospace Corporation personnel have decades of experience working with the sponsoring spacecraft organization and building space science instrumentation including data processing units and spacecraft interfaces for numerous space instruments; for TWINS they will perform these DPU and interface functions.

The project organization chart is shown in Figure 4.1. The P.I. will be assisted by a Project Manager (PM) and a small group of experienced engineers and scientists in the day-to-day management of the TWINS program. Within each of the three institutions building hardware, a single point of contact will interface with the LANL project management team (see Table 4.1). All co-investigators will serve on the TWINS science team, providing scientific and technical support for the TWINS investigation. Dr. J. Burch, IMAGE PI and Co-I on this proposal, will provide technical and scientific coordination between the IMAGE and TWINS investigations. A dedicated subset of the TWINS Co-Is, under the leadership of Dr. R. Skoug, will comprise the TWINS Outreach Team. The TWINS management team proposes to utilize the NASA/GSFC cost/progress reporting and review process to review cost, schedule, and technical performance. Our management team has been intentionally streamlined to ensure quick and accurate communications, reduce management cost, and provide our team members with clear and simple lines of authority and communications.

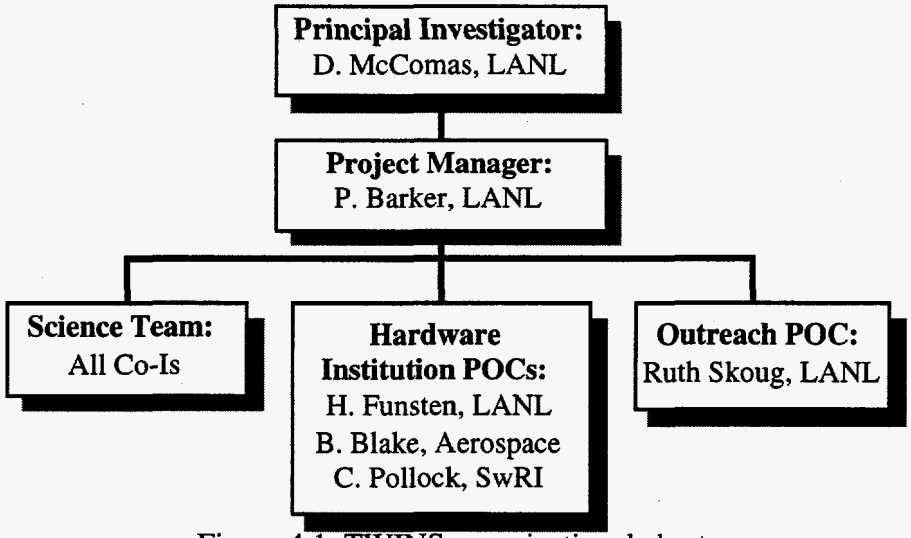

Figure 4.1 TWINS organizational chart.

LANL will provide funding to all TWINS team members through subcontracts. Each subcontractor will report costs to LANL using the established NASA 533 cost reporting process. These costs will then be rolled up into LANL total costs, and submitted to GSFC. LANL will be responsible for the technical and financial performance of all TWINS team members.

LANL will develop an integrated statement of work (SOW) describing all subsystems and deliverable items. In addition, the parameters of each subsystem will be described in an integrated interface specification document (ISD), which will be updated as needed throughout the project.

4.2 Decision-making Process

Activities will be coordinated with the PM and the PI through management team meetings concerning the status of activities, problem resolution, and resource allocation. These meetings will occur at least monthly and more frequently as needed to address any critical issues or problems. We will report results to the Explorer Project Office at the end of each of these management team meetings.

We will utilize LANL's strong system engineering support to identify and solve any instrument issues. Systems trade studies will be managed with the goal of obtaining the highest probability of success and best science within contract resource limitations. The PI will be responsible for making final decisions relating to the results of trade studies. Close coordination among the three hardware institutions will be maintained throughout the systems engineering process.

4.3 Team Organization and Responsibilities

Table 4.1 contains a list of the institutions that will carry the responsibility for the development of the TWINS flight hardware and software. Each team member is experienced and equipped to carry out the hardware development responsibilities. The infrastructure exists at each institution to support the performance assurance, fabrication, integration, functional and environmental testing, and personnel training necessary to insure high reliability flight equipment.

Table 4.1. Organizational responsibilities of hardware institutions.

Institution	Responsibilities	Point of Contact	Related Experience
LANL	PI institution, System level testing, actuator	D. McComas	Ulysses/SWOOPS PI, IMAGE/MENA Co-I, ACE/SWEPAM PI, Cassini/IMS PI
	PM	P. Barker	ACE/SWEPAM PM DS-1/PEPE LANL-PM
	Outreach	R. Skoug	Sounding Rocket Proj. Sci.
Aerospace Corporation	DPU, S/C Interface, GSE, flight software, S/C integration and test, Mission operations	B. Blake	Polar/CEPPAD PI, Polar/CAMMICE Co-I, Sampex Co-I, Ulysses/EPAC Co-I
LANL	Sensor heads, Calibration	H. Funsten	Cassini/IMS, IMAGE/MENA, DS1/PEPE
SwRI	Sensor Electronics, HVPS, Actuator control	C. Pollock	IMAGE/MENA PI, POLAR/TIDE Co-I

LANL will work with GSFC Performance Assurance (PA) engineers to develop a TWINS PA Requirements document. We will then work with the two hardware team members to develop PA implementation plans. The team will establish and implement an integrated Configuration Mgt. (CM) plan. Each team member will be subject to a CM audit. LANL will be responsible for strict enforcement of interface configuration control between the TWINS subsystems. Interfaces between TWINS and the spacecraft will be documented and controlled as part of the ISD.

4.4 Risk Management

Throughout the TWINS development program we will apply the classic elements of risk management: identification, avoidance, and control. Although we generally associate risk control with the use of unproven technologies, it can include schedule, cost control, or instrument performance risk. TWINS relies only on proven technologies, which have been developed for previous missions such as IMAGE (MENA) and Cassini (the CAPS Actuator), and many years of experience working with the spacecraft organization which is providing the ride of opportunity and with their missions. Our approach to risk is based on early identification of any risk areas, which will be assessed during Phase A.

4.5 Schedule and Scheduling System

Figure 4.2 shows a top-level development schedule for the TWINS investigation. Each of the three hardware organizations will be responsible for maintaining detailed schedules for their respective activities. The PM will integrate each of these individual schedules into a master TWINS schedule. Each month the respective schedules will updated and the integrated schedule will be reported to GSFC. Not only will the process just described produce a complete and accurate schedule, but it will also highlight both schedule and resource conflicts.

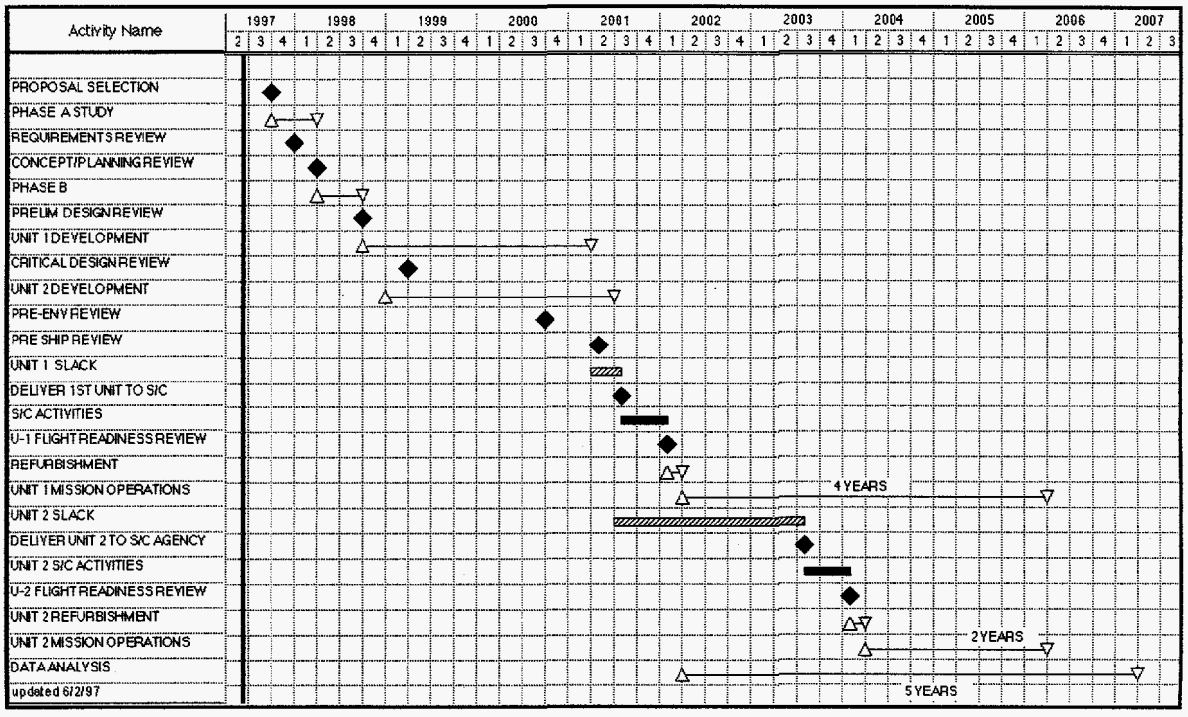

Figure 4.2 TWINS top-level schedule

5.0 COST AND COST ESTIMATING METHODOLOGY

Cost estimating was performed by the "bottom-up" approach consisting of: 1) defining the required work and deliverables in a work breakdown structure, 2) developing a schedule based on S/C delivery and project start dates, 3) estimating the resources needed to accomplish the tasks defined in the WBS according to the schedule, and 4) reviewing the cost model by comparing the estimates to similar recent and current flight hardware development projects. Labor estimates were derived from experience with the IMAGE/MENA and other recent programs, and the fabrication estimates were derived using recent MENA, Lunar Prospector and PEPE hardware fabrication data. Similar recent hardware development efforts were used as guidelines by Aerospace and SwRI. Appendix 2 includes the detailed WBS used for TWINS costing.

Table 5.1 gives the total NASA costs for the TWINS mission. This budget provides for the delivery and flight of TWINS instruments on two mission of opportunity spacecraft for a cost of approximately $10M (Phase A/B/C/D), and also includes science phase costs of approximately $5M (Phase E). Because of this opportunity, TWINS is able to provide stereo images of the magnetosphere for a fraction of the cost of a dedicated multipoint imaging mission. Note that the development and fabrication of the two instruments are done simultaneously. Phase E thus begins as soon as S/C-1 is launched. A small amount of additional Phase C/D funds are required at the time of the S/C-2 launch. The Education and Outreach budget has been calculated at 2% of all Phase A/B/C/D/E costs, excluding contingency funds.

Table 5.1 TWINS mission NASA costs.

Item	FY98	FY99	FY00	FY01	FY02	FY03	FY04	FY05	FY06	FY07	Total (Real Yr.)	Total (FY1997)
PHASE A	245										245	236
PHASE B/C/D	1901	3064	1619	1959	1832	0	696	0	0	0	11070	9809
Instrument A	1653	2665	1408	1703	780	0	165	0	0	0	8373	7527
Instrument B	0	0	0	0	0	0	0	0	0	0	0	0
Spacecraft	0	0	0	0	0	0	0	0	0	0	0	0
MSI&T	0	0	0	0	813	0	440	0	0	0	1253	1003
Grnd Data Syst Dev	0	0	0	0	0	0	0	0	0	0	0	0
Launch Services	0	0	0	0	0	0	0	0	0	0	0	0
Contingency	248	400	211	256	239	0	91	0	0	0	1444	1280
PHASE E	0	0	0	0	543	1389	1453	1677	892	452	6405	4806
OUTREACH	38	53	28	34	43	28	41	34	18	9	326	272
												0
NASA Mission Cost	2184	3118	1647	1993	2417	1417	2190	1710	910	461	18046	15122
							Mission Totals				18046	15122

OUTREACH = 2% of Phases A/B/C/DE costs

APPENDIX 3 STATEMENT OF WORK

The Space Physics Team at the Los Alamos National Laboratory, in collaboration with five other institutions, proposes to design, develop, deploy, and operate two neutral atom imaging instruments for the purpose of collecting and analyzing data to conduct a scientific investigation of the earth's magnetosphere. This, the TWINS project, will provide the first stereo investigation of the magnetosphere, contributing new insight into its make-up and processes.

With the study and preliminary design phases occurring in FY1998, and development phases in FY1999-2002, the project will launch the first instrument aboard a non-NASA U.S. government opportunity mission in FY2002. This instrument will have a minimum lifetime of four years. The second instrument will follow on a sister mission in FY2004 with a nominal lifetime of two years, thereby providing a stereo investigation during the second half of FY2004, all of FY2005 and the first half of FY2006.

LANL will have overall responsibility for the TWINS project. This includes the coordination of: project management and administrative support, reliability, quality assurance, and safety activities, science support, systems support (including reviews and interface definition), overall design and mission planning, system integration, testing and calibration, and data analysis system design and planning, In addition, specific LANL hardware tasks include development of the sensor housing, collimators, re-closable door assembly, gratings, start foil assembly, actuators, and geocoronal imager, and sub-system integration.

The effort will include collaboration of five other development teams from the following institutions: the Aerospace Corporation, providing DPU and ground support test equipment development, and S/C system integration; the Southwest Research Institute, providing detector, high voltage power supply, and front end electronics development; and the Applied Physics Laboratory, the University of Southern California, and West Virginia University teams providing UV filtering, neutral atom imaging, and charged particle rejection expertise. All institutions will play a role in the data analysis and science portion of the investigation.

The instrument development effort will use the technologies presently being developed by SwRI, LANL, USC, and WVU for the MIDEX IMAGE/MENA instrument and the similar S/C systems coordination experience gleaned from the LANL/Aerospace Corp. collaboration on the LENA Prototype project.

A top level schedule and work breakdown structure for the proposed TWINS Project are attached. The schedule includes dates and time periods for all project phases and includes reviews required by the project. The WBS includes a breakdown of all major activities and lists the institution with primary responsibility.

TWINS PROJECT SCHEDULE

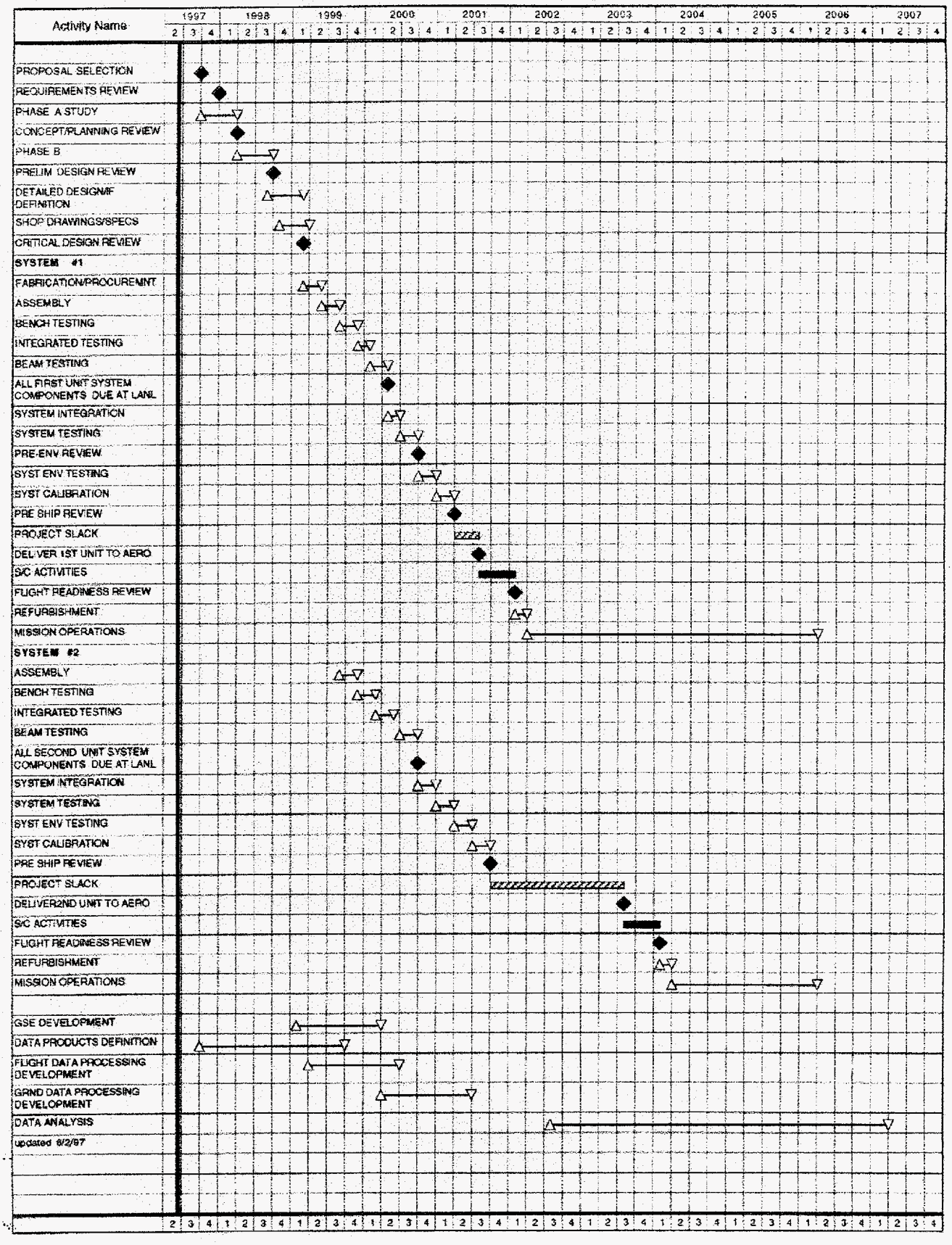

Work Breakdown Structure For The Twins Proposal

1.0 Project Management/Administrative Support (LANL)
- 1.1 NASA & Co-I Institution Interface
- 1.2 *Progress Reports
- 1.3 *Cost Reports
- 1.4 Program Support
- 1.5 Contract maintenance
- 1.6 Project Leadership

2.0 R&QA/Safety Activities(LANL)
- 2.1 QA Program Review/Negotiation - (meet or exceed NHB5300.4 specs.)
- 2.2 QA Report/Alert/etc. Activities
- 2.3 Safety Assessment/Report/Activities

3.0 Science Support (LANL)
- 3.1 Science Support
  - 3.1.1 Aero Support
  - 3.1.2 APL Support
  - 3.1.3 LANL Support
  - 3.1.4 SwRI Support
  - 3.1.5 USC Support
  - 3.1.6 WVU Support
- 3.2 Data products definition
- 3.3 Derive De-convolution Algorithms
- 3.4 DPU Science Data Handling Support
- 3.5 Instrument Operating Modes Definition
- 3.6 Data Processing Station Set up/Testing/Maintenance
- 3.7 Instrument Operations
- 3.8 Data Analysis
- 3.9 *Scientific Papers

4.0 Systems Support (LANL)
- 4.1 Mechanical Interface Definition - Development of the *Interface Control Document
- 4.2 Electrical Interface Definition - Development of the *Interface Control Document
- 4.3 Review Support
  - 4.3.1 Requirements Review (semiformal)
  - 4.3.2 Concept Review (semiformal)
  - 4.3.3 Preliminary Design Review (formal)
  - 4.3.4 Critical Design Review (formal)
  - 4.3.5 Pre-environmental Review (formal)
  - 4.3.6 Pre-ship Review (formal)
  - 4.3.7 Flight Readiness Review (formal) (#1 and #2)
- 4.4 *Provide Coatings for Parts for Other Agencies As Needed

5.0 *Sensor housing (faceplate, walls, baseplate, purge system, light seal, pump out baffle/system, grating interface, HV interface) (LANL)
- 5.1 Electro-optical Analysis (of detector system for mapping of secondary electrons)
- 5.2 Design
- 5.3 Fabrication

6.0 *Collimator (bookends, plates, mesh, HV interface)(LANL)
- 6.1 Design
- 6.2 Fabrication

6.3 Function/Fit check
6.4 Cleaning/Coating/Assembly
6.5 Test (HV), Test (charged particle rejection), Angle Response
6.6 Characterize

7.0 *Re-closable Door Assembly (LANL)
7.1 Design
7.2 Fabrication/Purchase Parts
7.3 Function/Fit Check
7.4 Cleaning/Coating/Assembly
7.5 Test

8.0 *Gratings (gratings, holders, grating assemblies, start foil interface) (LANL)

8.1 Specify and Purchase prototype Units
8.2 Test PT Units
8.2.1 Mechanical/Acoustical Vibration Testing
8.2.2 Characterize/Test (UV transmission)
8.2.3 Characterize/Test (particle transmission)
8.3 Specify/Purchase Flight Units
8.4 Design, Fabricate, and Assemble Grating Mounts
8.5 Mount/assemble/Fit Flight Gratings & Mounts
8.6 Test FM units
Same as 8.2

9.0 *Start Foil Assembly (foils, holders, acceleration grid w/holder, grating mount interface) (LANL)
9.1 Raytraces
9.2 Designs/Fabricate Foil Mounts
9.3 Procure and Mount Foils
9.4 Characterize For Holes/Defects
9.5 Mechanical/Acoustical Vibration Testing
9.6 Perform UV Lifetime Tests

10.0 Foil/Gratings/Door/Collimator/Sensor Integration (LANL)
10.1 Fit Check/Assembly
10.2 Bench Test
10.3 Beam Test

11.0 *Electronics (SwRI)
11.1 Time of Flight Electronics
11.2 Time to Digital Converter
11.3 Position Electronics
11.4 Pulse Height Analysis Electronics
11.5 Actuator Electronics Design
11.6 High Voltage Power Supply
11.7 Mechanical Structure

12.0 *Detector Assembly(SwRI)
12.1 Grid/Holder
12.2 Micro Channel Plate/Holder
12.3 Anode/Holder
12.4 Charge Amp
12.5 Mech/Ele Interface
12.6 MCPs and burn-in

13.0 Spacecraft Items (AERO)
- 13.1 S/C Interface
- 13.2 *Low Voltage Power Supply

14.0 *Data Processing Unit (AERO)
- 14.1 Command Logics
- 14.2 Housekeeping Monitors
- 14.3 High Voltage Controllers
- 14.4 Modes of Operation
- 14.5 Flight software
- 14.6 Data Processing
- 14.7 Data storage
- 14.8 Telemetry Interface
- 14.9 Actuator Electronics fabrication and test
- 14.10 Mechanical Structure

15.0 *Ground Support Equipment (AERO)
- 15.1 Electronic System Test Equipment
- 15.2 Mechanical Support Equipment

16.0 *Actuators (LANL)
- 16.1 Electrical parts supplied by SwRI to VTT
- 16.2 Actuator units purchased from VTT (use Cassini design)

17.0 Integrated Sensor Testing Support (LANL)
- 17.1 Test (HV)
- 17.2 Test (charged particle rejection)
- 17.3 Test (ENA detection, including position sensing and TOF)
- 17.4 Test (UV rejection)

18.0 Environmental Testing (LANL)
- 18.1 Mechanical Integration
- 18.2 Electrical Integration
- 18.3 Vibration Testing
- 18.4 Acoustic Testing
- 18.5 Thermal Vacuum Testing

19.0 Calibration (LANL)
- 19.1 Angular (Polar &Azimuthal) Response
- 19.2 Energy Response
- 19.3 Resolution
- 19.4 G-Factor

20.0 S/C Integration/Test activities (AERO)
- 20.1 S/C System Testing Support as Needed
- 20.2 Refurbishment???
- 20.3 Reintegration???
- 20.4 Launch preps
- 20.5 L+30 Turn On and Check Out

21.0 Outreach (LANL)
- 21.1 Web Site Program
- 21.2 Direct Involvement
  - 21.2.1 General Public Programs
  - 21.2.2 School Programs

22.0 *Ly-α Geocoronal Imager System
- 22.1 Imager (LANL) (purchase existing units)
- 22.2 CEM HVPS (SwRI)

* Deliverables

APPENDIX 4 REFERENCES

Baker, D. N., E. W. Hones, Jr., D. T. Young, and J. Birn, The possible role of ionospheric exygen in the initiation and development of plasma sheet instabilities, *Geophys. Res. Lett.*, **9**, 1337, 1982.

Blake, J. B. The energetic radiation environment in a highly elliptical (Molniya) orbit, in *Proceedings of the ESA Workshop on Space Environment Analysis, ESA WPP-23,* ESTEC, Noordwijk, The Netherlands, 1990.

Blake, J. B., D. N. Baker, N. Turner, K. W. Ogilvie, and R. P. Lepping, Correlation of changes in the outer-zone relativistic-electron population with upstream solar wind and magnetic field measurements, *Geophys. Res. Lett.*, **24**, 927, 1997.

Burch, J. L., et al., Sun-Earth Connection Roadmap: Strategic Planning for the years 2000-2020, 1997.

Chase, C. J., and E. C. Roelof, Extracting evolving structures from global magnetospheric images via model fitting and video visualization, *Johns Hopkins APL Technical Digest,* **16**, 111, 1995.

Fennell, J. F., J. B. Blake, J. L. Roeder, R. Sheldon, and H. E. Spence, Tail lobe and open field line region entries at mid to high latitudes, *Adv. Sp. Res., in press*, 1997.

Fok, M.-C., T. E. Moore, and M. E. Greenspan, Ring current development during storm main phase, *J. Geophys. Res.*, 101, 15311, 1996.

Funsten, H. O. and M. Shappirio, Sputtering of thin carbon foils by 20 keV and 40 keV Ar^+ bombardment. *Nucl. Instrum. and Meth. B, in press*, 1997.

Funsten, H. O., B. L. Barraclough, and D. J. McComas, Pinhole detection in thin foils used in space plasma diagnostic instrumentation. *Rev. Sci. Instrum.*, **63**, 4741, 1992a.

Funsten, H. O., D. J. McComas, and B. L. Barraclough, Thickness uniformity and pinhole density analysis of thin carbon foils using keV ions. *Nucl. Instrum. and Meth. B*, **66**, 470, 1992b.

Funsten, H. O., D. J. McComas, and B. L. Barraclough, Ultrathin foils used for low energy neutral atom imaging of planetary magnetospheres. *Optical Engineering*, **32**, 3090, 1993.

Funsten, H. O., D. J. McComas, and M. A. Gruntman, Neutral Atom Imaging: UV Rejection Techniques, in *AGU Monograph: Measurement Techniques for Space Plasmas*, Eds. J. Borovsky, R. Pfaff, and D. T. Young, *in press*, 1997.

Funsten, H. O., D. J. McComas, and E. E. Scime, Low energy neutral atom imaging for remote observations of the magnetosphere. *J. Spacecraft and Rockets*, **32**, 899, 1995.

Funsten, H. O., D. J. Suszcynsky, R. W. Harper, J. E. Nordholt, and B. L. Barraclough, Effect of local electric fields on microchannel plate detection and spatial resolution. *Rev. Sci. Instrum.*, **67**, 145, 1996.

Grande, M., J. F. Fennell, S. Livi, B. Kellett, C. Perry, P. Anderson, J. L. Roeder, H. E. Spence, T. Fritz, and B. Wilken, First POLAR and 1995-034 observations of the mid-altitude cusp during a persistent northward IMF condition, *Geophys. Res. Lett., in press*, 1997.

Gruntman, M. A., Extreme-ultraviolet radiation filtering by freestanding transmission gratings, *Appl. Opt.*, **34**, 5732, 1995.

Gruntman, M. A., Transmission grating filtering of 52-140 nm radiation, *Appl. Opt.*, **36**, 2203, 1997.

Henderson, M. G., G. D. Reeves, H. E. Spence, R. B. Sheldon, A. M. Jorgensen, J. B. Blake, and J. F. Fennell, First energetic neutral atom images from Polar CEPPAD/IPS, *Geophys. Res. Lett.*, **24**, 1167, 1997.

Hesse, M., D. Mitchell, E. Roelof, B. Mauk, D. McComas, H. Funsten, and J. Birn, Neutral atom imaging of the plasma sheet: Measurement predictions, *Geophys. Res. Lett., in press*, 1997.

Jordanova, V. K., L. M. Kistler, J. U. Kozyra, G. V. Khazanov, and A. F. Nagy, Collisional losses of ring current ions, *J. Geophys. Res.*, **101**, 111, 1996.

Joselyn, J. A., J. B. Anderson, H. Coffey, K. Harvey, D. Hathaway, G. Heckman, E. Hildner, W. Mende, K. Schatten, R. Thompson, A. W. P. Thomson, and O. R. White, Panel achieves consensus prediction of Solar Cycle 23, *EOS, Trans. Amer. Geophys. Union*, **78**, 205, 1997.

Lui, A. T. Y., H. E. Spence, and D. P. Stern, Empirical modeling of the quiet time nightside magnetosphere, *J. Geophys. Res.*, **99**, 151, 1994.

McComas, D.J., B.L. Barraclough, R.C. Elphic, H.O. Funsten III, and M.F. Thomsen, Magnetospheric Imaging with Low Energy Neutral Atoms, *Proceedings of the National Academy of Sciences, USA*, **88**, 9589, 1991.

McComas, D.J., H.O. Funsten, and E.E. Scime, Advances in low energy neutral atom imaging, in *AGU Monograph: Measurement Techniques for Space Plasmas*, Eds. J. Borovsky, R. Pfaff, and D. T. Young, *in press*, 1997.

Meier, R. R., Ultraviolet Spectroscopy and Remote Sensing of the Upper Atmosphere, *Space Sci. Rev.*, **58**, 1, 1991.

Mitchell, D.G., et al., INCA: The ion neutral camera for energetic neutral atom imaging of the Saturnian magnetosphere, *Opt. Eng.*, **32**, 3096, 1993.

Ngo, T., E. J. Snyder, W. M. Wong, R. S. Williams, and M. S. Anderson, O-atom etching of graphite in low-Earth-orbit, *Surface Science*, **314**, L817, 1994.

Ogawa, H. S., D. R. McCullin, D. L. Judge, and R. Korde, Normal incidence spectrophotometer with high-efficiency silicon photodiodes for absolute solar extreme-ultraviolet irradiance measurements, *Opt. Eng.*, **32**, 3121, 1993.

Rairden, R. L., L. A. Frank, and J. D. Craven, Geocoronal imaging with Dynamics Explorer, *J. Geophys. Res.*, **91**, 13613, 1986.

Ritzau, S. M., Ion induced electron emission from ultra thin carbon foils and nearly free electron metals, Ph.D. Dissertation, University of Virginia, May, 1997.

Roelof, E.C., Energetic neutral atom imaging of a storm-time ring current, *Geophys. Res. Lett.*, **15**, 652, 1987.

Roelof, E.C., Remote sensing of the ring current using energetic neutral atoms, *Adv. Space. Res.*, **9**, 195, 1989.

Roelof, E. C., ENA emission from nearly-mirroring magnetospheric ions interacting with the exosphere, *Adv. Space Res., in press*, 1997.

Roelof, E. C., and D. G. Sibeck, The magnetopause shape as a bivariate function of IMF B_Z and solar wind dynamic pressure, *J. Geophys. Res.*, **98**, 21421, 1993.

Roelof, E. C., B. H. Mauk, R. R. Meier, K. R. Moore, and R. A. Wolf, Simulations of EUV and ENA magnetospheric images based on the Rice convection model, in *Instrumentation for Magnetospheric Imagery II*, Ed. S. Chakrabarti, *Proc. SPIE*, **2008**, 202, 1993.

Schattenburg, M. L., R. J. Aucoin, R. C. Fleming, I. Plotnik, J. Porter, and H. I. Smith, Fabrication of high energy x-ray transmission gratings for AXAF, *Proc. SPIE*, **2280**, 181, 1994.

Scime, E. E., E. H. Anderson, D. J. McComas, and M. L. Scattenburg, Extreme-ultraviolet polarization and filtering with gold transmission gratings, *Appl. Opt.*, **34**, 648, 1995.

Wurz, P., M.A. Allig, P. Bochsler, A.G. Ghielmetti, E.G. Shelly, S.A. Fuselier, F.Herrero, M.F. Smith, and T.S. Stephen, Neutral atom imaging mass spectrograph, *Opt. Eng.*, **34**, 2365, 1995.